2010

Mineralization Potential of Electrospun PDO-nHA-Fibrinogen Scaffolds Intended for Cleft Palate Repair

Isaac Rodriguez
Virginia Commonwealth University

Virginia Commonwealth University

This is to certify that the thesis prepared by Isaac Anthony Rodríguez entitled Mineralization Potential of Electrospun PDO-nHA-Fibrinogen Scaffolds Intended for Cleft Palate Repair has been approved by his committee as satisfactory completion of the thesis requirement for the degree of Master of Science in Biomedical Engineering

Gary L. Bowlin, Ph.D., Director of Thesis, School of Engineering

Peter C. Moon, Ph.D., School of Dentistry

Hu Yang, Ph.D., School of Engineering

Gerald E. Miller, Ph.D., Chair of Biomedical Engineering, School of Engineering

Roselyn Hobson, Ph.D., Associate Dean for Graduate Studies, School of Engineering

Russell D. Jamison, Ph.D., Dean, School of Engineering

F. Douglas Boudinot, Ph.D., Dean of the School of Graduate Studies

May 2010

MINERALIZATION POTENTIAL OF ELECTROSPUN PDO-NHA-FIBRINOGEN SCAFFOLDS INTENDED FOR CLEFT PALATE REPAIR

A thesis submitted in partial fulfillment of the requirements for the degree of Master of Science in Biomedical Engineering at Virginia Commonwealth University.

by

ISAAC ANTHONY RODRIGUEZ
Bachelor of Science, University of Virginia, 2007

Director: GARY L. BOWLIN, PH.D.
Professor, Biomedical Engineering

Virginia Commonwealth University
Richmond, Virginia
May 2010

Acknowledgement

First of all I would like to thank Dr. Bowlin for giving me the chance to work in his lab. He has been an exceptional mentor always setting high goals for me. I also wanted to thank my advisors Dr. Moon and Dr. Yang for their support and guidance throughout this project. Special thanks to Dr. Moon for allowing me to use his equipment and lab space.

Bone tissue engineering is a field I was always interested in and this has been a great experience and opportunity. I want to acknowledge Dr. Parthasarathy Madurantakam who was the one who gave me the opportunity to work with him and trained me in the lab. Without his guidance I would not be where I am today. Special thanks to Rebecca Duffy who worked with me on this project and made this possible. I also want to thank my lab colleagues Dr. Scott Sell, Michael McClure, Patricia Wolfe, Koyal Garg, Jennifer McCool, Yas Maghdouri Moghaddam, and Anna Bulysheva for their assistance and for making the lab environment fun to work in.

Last but not least I would like to thank my family. None of this would be possible without their love and support. I specifically want to recognize my Mom (Becky), Dad (Jose), sister (Kayla), and stepmom (Kristi) for always believing in me and encouraging me to be the best. I also consider my fraternity, La Unidad Latina, Lambda Upsilon Lambda Fraternity, Inc. my family and want to thank my Hermanos for their support.

Table of Contents

Page

List of Tables

Page

List of Figures

Page

Abstract

MINERALIZATION POTENTIAL OF ELECTROSPUN PDO-NHA-FIBRINOGEN SCAFFOLDS INTENDED FOR CLEFT PALATE REPAIR

By Isaac Anthony Rodríguez, B.S.

A Thesis submitted in partial fulfillment of the requirements for the degree of Masters of Science in Biomedical Engineering at Virginia Commonwealth University.

Virginia Commonwealth University, 2010

Major Director: Dr. Gary L. Bowlin
Professor, Biomedical Engineering

The overall goal of this study was to identify mineralized scaffolds which can serve as potential alternatives to bone graft substitutes intended for cleft palate repair. The aim of this preliminary study was to evaluate the role of fibrinogen (Fg) and nano-hydroxyapatite (nHA) in enhancing mineralization potential of polydioxanone (PDO) electrospun scaffolds. Scaffolds were fabricated by blending PDO:nHA:Fg in the following weight ratios: 100:0:0, 50:25:25, 50:50:0, 50:0:50, 0:0:100 and 0:50:50. Scaffolds were immersed in different simulated body fluids for 5 and 14 days to induce

mineralization. The inclusion of fibrinogen induced sheet-like mineralization while individual fiber mineralization was noticed in its absence. Modified protocols of alizarin red staining and burn-out test were developed to quantify mineral content of scaffolds. After mineralization, 50:50:0 scaffolds were still porous and contained the most mineral. 50:25:25 scaffolds had the highest mineralization potential but lacked porosity. Therefore, it can be anticipated that these mineralized organic-inorganic electrospun scaffolds will induce bone formation.

.

CHAPTER 1 Introduction

Observed in approximately 1 in 700 live births, cleft lip (with or without cleft palate) is the most common congenital craniofacial birth defect in humans [1-3]. Cleft palate occurs when the palatal shelves do not fuse properly [4]. Current treatments for cleft palate involve surgeries which rotate adjacent soft tissue into the defect site and secondarily graft hard tissue into the cleft defect [5]. The most common hard tissue graft is an autograft, whereby bone is taken from the patient's own body and reimplanted into the defect site. Autologous bone grafts harvested from patient donor sites are osteoconductive (provide a scaffold where bone cells can proliferate), osteoinductive (induce proliferation of undifferentiated cells and their differentiation into osteoblasts), and osteogenic (provide a reservoir of skeletal stem and progenitor cells that can form new bone) [6]. Autografts are the best material for bone repair because of their supreme histocompatibility without the risk of disease transfer. However, their limited availability, additional invasive surgery, and donor site morbidity are all drawbacks which encourage the development of alternative bone substitutes [6-11].

The most frequently used donor site for cleft palate repair is cancellous iliac bone. Alternative donor sites have been explored [12, 13], however even these suffer the same drawbacks mentioned above. The field of tissue engineering "aims to restore function to or replace damaged or diseased tissues through the application of engineering and biological

principles" [5]. Using polymeric scaffolds and tissue engineering techniques, the use of autologous bone grafts can potentially be eliminated during cleft palate repair.

Project Synopsis

The aims of this study were to (i) evaluate the role of fibrinogen in enhancing the mineralization potential of PDO-nHA blended electrospun scaffolds, (ii) identify a scaffold composition for optimal mineralization, and (iii) evaluate the mineralizing potential of different simulated body fluids (SBF) on electrospun scaffolds. This study will further help evaluate the potential of these electrospun scaffolds as alternative substitutes to autologous bone grafts.

Electrospun scaffolds were fabricated using polydioxanone (PDO), nanocrystalline hydroxyapatite (nHA), and Fibrinogen (Fg). PDO and Fg were dissolved in 1,1,1,3,3,3 hexafluoro-2-propanol (HFP) at 100 mg/ml. Different scaffold types were fabricated by blending PDO:nHA:Fg in the following weight ratios: 100:0:0, 50:25:25, 50:50:0, 50:0:50, 0:0:100 and 0:50:50. Conventional (c), revised (r), ionic (i), and modified (m) simulated body fluids were prepared by modifying a published protocol. 10 mm diameter discs were punched from the electrospun sheet and incubated in c, r, i, or m-SBF for 5 and 14 days at 37°C and 5% CO_2 atmosphere. SBF solutions were prepared and replenished every 5 days.

After 5 and 14 days, scaffolds were removed and rinsed with DI water to remove any unbound minerals and analyzed for mineral content using modified protocols for alizarin red staining (ARS) and burn-out method. Scanning electron microscopy (SEM) was used to analyze scaffold topography before and after mineralization. This study did not

focus on analyzing mechanical properties of the scaffolds, but rather the potential of the scaffolds to induce mineralization ultimately supporting bone ingrowth.

CHAPTER 2 Background Information

Bone: Structure and Remodeling

Bone is a natural composite of collagenous organic matrix reinforced by an inorganic mineral phase of hydroxyapatite (HA) whose structure is ultimately responsible for its functional properties. Other components of bone include calcium phosphates, water, proteins, etc. [14]. Natural bone is a complex and highly organized structure of parallel collagen nanofibrils, and carbonated apatite (HA nanocrystals) located within the fibrils and precipitated on their surface [14, 15]. These hydroxyapatite nanocrystals can be either platelet or spindle shaped and up to about 200 nm long which creates a large surface area for effective mineral exchange [16]. Type I collagen is the main organic component of mineralized extracellular matrix (Figure 1). The extracellular matrix (ECM) is the foundation upon which minerals are deposited. Ultimately, the biomechanical properties and biological function is attributed to this organic-inorganic nanocomposite bone ECM [17]. Our lab developed a method to successfully incorporate nHA within polymeric electrospun nanofibers to mimic the structure of native bone ECM [18].

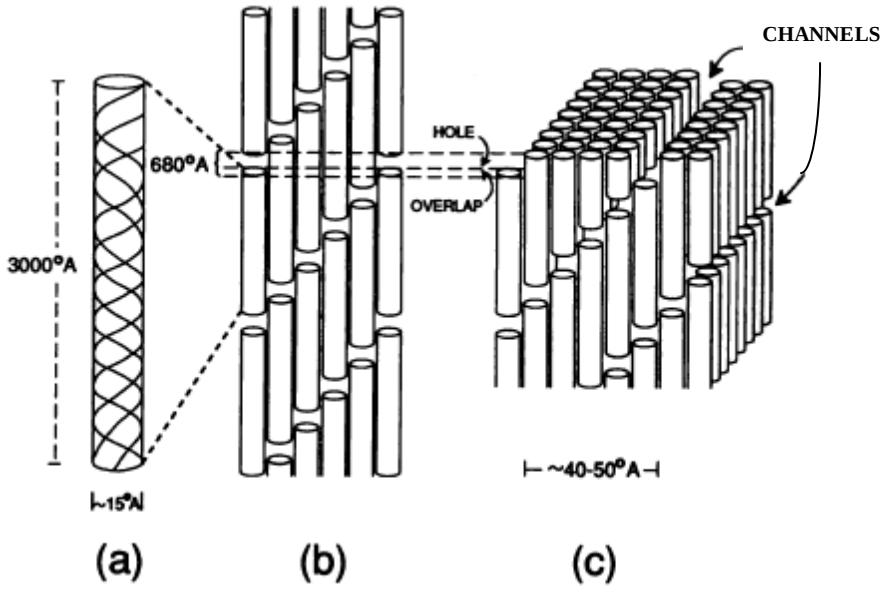

Figure 1: Illustration of the structure of type I collagen. a) Single triple helical molecule. b) 2-dimensional view of the staggered array orientation of part of a collagen fibril. C) 3-D section of the structure showing triple helical molecules arranged such that adjacent hole zones and channels or grooves are created [15].

Bone undergoes continuous yet subtle remodeling in order to achieve its function. The mineral components, such as calcium phosphates and hydroxyapatites are responsible for the hardness of bone. The toughness and visco-elasticity is attributed to the soft organic collagenous matrix [19]. At the cellular level, osteoblasts reside on the surfaces of bone and are involved in the formation and organization of bone ECM (Figure 2). Osteoblasts are also responsible for bone mineralization and producing the organic components of the ECM (mainly type I collagen). Osteoclasts are cells which adhere to the bone surface and are responsible for mineral dissolution and the degradation of the organic phase (bone resorption) [17].

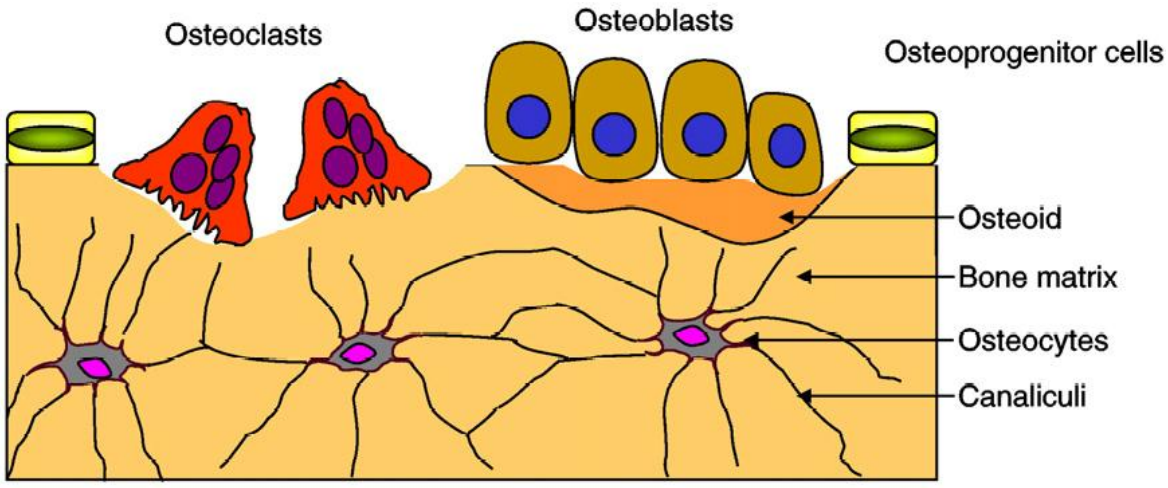

Figure 2: Diagram of the structure of bone at a cellular level [17].

Mineralization of bone first occurs at nucleation sites located within the hole zone regions of the organic matrix of bone (collagen fibrils). This region is a volume of space where mineral crystals (calcium phosphates, Ca-P) are deposited from the extracellular fluid. Since mineralization occurs in these hole zones, it suggests that the three-dimensional geometry and the composition of the fibrils (mineral-filled collagen) are factors in mineralization. Specifically suggesting that nucleation sites are located in the collagen fibrils within the hole zone regions. This initial nucleation process occurs at independent sites within the collagen fibrils and does not damage or disrupt the matrix structure. After the initial nucleation, there is continuous formation of Ca-P crystals due to secondary nucleation of the already formed crystals. Also during this stage, primary nucleation sites within the hole zone which did mineralize are still able to nucleate Ca-P crystals. Throughout the mineralization process calcium phosphates undergo a phase transformation from a solution (extracellular fluid) to a solid phase (Ca-P crystals). It is

important to note that the increase in mineralization is due to the increase in the number of crystals rather than the increase in the size of the crystals already formed [20]. This native mineralization process is the underlying principles behind biomimetic mineralization described later.

Mineralization of a polymer scaffold occurs in the same manner as described above for native bone. Mineral nucleation occurs first on the polymer surface and then mineral crystals grow and multiply on the nucleated mineral [21].

Bone Tissue Engineering

Tissue Engineering focuses on developing viable substitutes that are able to repair and regenerate the functions of damaged tissue [22]. Specifically, bone tissue engineering requires a scaffold to temporarily support cell adhesion and direct their growth into bone tissue until the scaffold is completely replaced by the new tissue [23]. Since cellular growth depends on the characteristics of the scaffolding system, it is important to fabricate scaffolds that mimic the structure and composition of natural bone ECM [24].

Several scaffold fabrication techniques have been developed for tissue engineering applications. Some of these include freeze-drying [14], solvent casting/particulate leaching [21, 25], gas foaming/particulate leaching [7, 9, 11], plates/meshes [26], solvent casting/salt leaching [27], salt leaching/solid-liquid phase separation [28], and electrospinning [10, 17, 24, 29-35]. Important factors in the success of bone tissue engineering scaffolds include biocompatibility, degradability, osteoconductivity, and mechanical stability. Biocompatibility and degradability can be controlled by the

polymer(s) used. Osteoconductivity and mechanical stability can be potentially be enhanced by the growth of a bonelike mineral (BLM) on the scaffold surface prior to cell seeding [25].

Polymers (both natural and synthetic) are a promising category of potential biomaterials used for bone tissue engineering [6]. Synthetic polymers have been specifically fabricated for medical applications because they are versatile and free of potential contamination [36]. The advantage of using synthetic polymers for scaffolding is that they are able to undergo chemical modifications in order to improve cell adhesion, cell function, and mineralization. However, synthetic polymers generally lack bioactivity without these modifications which led to interest in developing composite scaffolds combining osteoconductive materials with polymer-based materials [6]. Composite organic-inorganic scaffolds have the potential to satisfy the complex scaffold designs criteria such as material composition, architecture, structural mechanics, surface properties, and degradation properties and products [19].

Natural polymers attract special interest in tissue engineering since they are biocompatible, biodegradable, and natural substrates where cells can attach, proliferate, and function [37]. Due to its excellent bioactivity, biocompatibility, ability to induce cellular interaction and subsequent scaffold remodeling, fibrinogen is one such natural biopolymer of interest for tissue engineering [35, 38, 39]. Fibrinogen is a highly abundant plasma protein (340 kDa, globular) and consists of six polypeptide chains: 2Aα, 2Bβ, and 2 γ [40]. Fibrinogen functions as the main structural component in clot formation and wound repair [41, 42]. In addition to its role in clotting, fibrinogen is a protein which has

the capacity to bind a variety of molecules [38]. This property is of interest when evaluating the mineralization potential of fibrinogen blended scaffolds since it may provide more nucleation sites for mineral deposition. Previous studies have reported on the use of electrospun fibrinogen scaffolds for tissue engineering applications [35, 38, 39, 43]. However, the potential of electrospun fibrinogen scaffolds for bone tissue engineering has yet to be explored.

There has been widespread use of calcium phosphates (such as hydroxyapatites) for bone tissue engineering applications [7]. The major advantages of hydroxyapatites include (i) it is the major inorganic component of bone matrix, (ii) they have affinity to many adhesive proteins, and (iii) they are osteoconductive materials directly involved in bone cell differentiation and mineralization process [19, 34]. Even though inorganic HA materials have many advantages, they have limited use as tissue engineering scaffolds because they are brittle [30]. However, combining the bone-bioactivity of the inorganic materials with the structural integrity of the organic polymers introduces an organic-inorganic composite scaffold specifically tailored for bone tissue engineering.

Hydrophobic biomaterials support bone regeneration by promoting adsorption and retention of proteins (such as fibrinogen and fibronectin) that positively influence cell adhesion [44]. In addition, calcium-based ceramics undergo a phase transformation and precipitate on the surfaces as Ca-P crystals. This sequence of events leads to the formation of a carbonate-containing BLM layer on the surface which enhances osteoconductivity and is essential in creating a bond with the living host bone [45-47].

Biomimetic Mineralization

As previously mentioned, a BLM layer formed on the surface of biomaterials is an essential requirement for the material to bond to the living bone and enhance osteoconductivity. In 1990, Kokubo et al. developed an acellular solution (SBF) with ionic concentrations approximately equal to those of human blood plasma. The most commonly used SBF is conventional (c-SBF). Oyane et al. revised the c-SBF and prepared new SBFs that were closer to the ionic concentration of blood plasma. The SBFs developed were revised (r-SBF), ionic (i-SBF), and modified (m-SBF) [48].

SBF is used to induce mineral nucleation creating a BLM layer on the surface of materials [49]. This technique can be used for complex porous scaffolds since the apatite crystals are generated from an aqueous solution. Immersion of scaffolds in SBF is an easy task and does not require any special equipment. It has been found that the BLM (carbonated hydroxyapatite) layer generated resembles natural bone mineral in its nano-crystal size and low crystallinity [28]. SBF has been widely used for biomimetic BLM coating on bioinert materials to directly mimic the process of mineralization in native bone and to predict the *in vivo* bioactivity of the material [11, 18, 21, 25, 26, 29, 31, 33]. It has been found that if a material is able to form a BLM layer in short periods when immersed in SBF, then it will bond to living bone in short periods [50].

Electrospinning

In order to achieve cell attachment, growth, and tissue regeneration in three-dimension, scaffolds should be engineered to be porous (with interconnected network) and have a large surface area [24, 25, 29, 51]. Fabricating scaffolds that mimic the nanostructure and chemical composition of bone ECM is a promising option for bone tissue engineering [24]. Electrospinning is a scaffold fabrication technique which is economical, reliable, and simple. It is an easy method which can be used to create ECM mimicking scaffolds with nanofibers, high surface area, high porosity, and an interconnected pore network. It can also be used to control and modify the microstructure of the porous nanofibrous scaffolds [29, 31]. As previously mentioned, the first step of bone mineralization is nucleation of Ca-P crystals within the porous regions of the collagenous organic matrix. The large surface area and high porosity of electrospun scaffolds provide an ideal environment for primary nucleation suggesting that electrospun scaffolds can serve as effective ECM analogues for mineralization.

In the electrospinning process, a polymer solution is drawn into a syringe with a blunt needle tip. A static electric field is created by applying a large electric potential to the needle tip which is separated by some distance from a grounded mandrel target. When the electric potential reaches a critical level, the surface tension of the polymer solution at the needle tip is overcome creating a fine polymer jet of entangled polymer chains. As the polymer jet travels towards the grounded rotating mandrel, the solvent evaporates creating

a dry deposition of fibers. This fibrous structure that is collected on the mandrel is a non-woven mat that can be used as a scaffold for tissue engineering [31, 39, 43, 52].

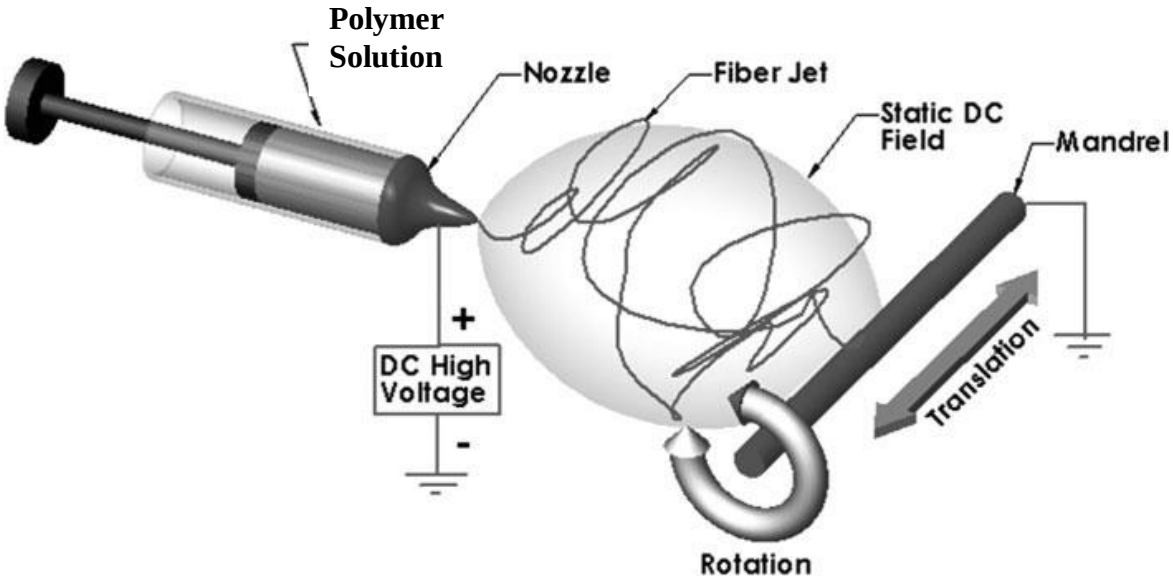

Figure 3: Diagram of the electrospinning process [39].

As previously mentioned, electrospinning is a simple process that allows the tissue engineer to control and modify several different characteristics of the ECM mimicking scaffolds. Fiber diameters can be controlled by varying the concentration and composition of the polymer solution; larger fiber diameters are observed as the concentration of the polymer solution increases. Scaffold thickness is directly related to the volume of polymer solution loaded in the syringe. Fibers can be randomly oriented or aligned depending on the rotation speed of the mandrel. A low rotation speed will result in a scaffold with randomly oriented fibers, while a high speed will create aligned fibers. Scaffold shape can also be controlled depending on the shape of the mandrel (rectangular, cylindrical, etc.)

[52]. Other properties of the scaffold can be controlled and optimized by altering electrospinning parameters such as the gauge of the needle tip, voltage applied, and the air gap distance (distance between needle tip and mandrel).

CHAPTER 3 Materials and Methods

Electrospinning

Electrospun scaffolds were fabricated with varying ratios of polydioxanone (PDO, Ethicon, Inc., NJ), Fibrinogen (Fraction 1, Type 1-S from bovine plasma, Sigma Aldrich, Co.), and nanocrystalline hydroxyapatite (nHA, Aldrich). PDO and Fg were dissolved in 1,1,1,3,3,3 hexafluoro-2-propanol (HFP, TCI America) at 100mg/ml. nHA was added as a wt % of the polymer and sonicated for 10 minutes on pulse mode (on: 50 s, off: 10 s) at 38% maximum amplitude using a Cole-Palmer Ultrasonic Processor sonicator (model CPX 750). Sonicating was necessary to ensure proper dispersal of the mineral since nHA sedimented in HFP. To this sonicated solution, a known amount of polymer was added to attain the final concentration. It has been shown that by using this method of preparing polymer-nHA solutions, nHA is successfully incorporated within the composite scaffold [18]. Different scaffold types were fabricated by blending PDO:nHA:Fg in the following ratios: 100:0:0, 50:25:25, 50:50:0, 50:0:50, 0:0:100 and 0:50:50. Fibrinogen solutions were made with a 90% by volume solution of HFP and 10% by volume of 10x minimal essential medium (MEM, Sigma Aldrich, Co.). Solutions were left for 24 hours on a shaker plate to ensure that all of the Fg dissolved to form a homogeneous solution [52]. In order to achieve PDO-Fg blended scaffolds, calculated volume of Fg solution was transferred to a

known volume of PDO solution, briefly vortexed, and placed on shaker for 5 minutes prior to electrospinning. All solutions were loaded into a 5mL syringe (Luer-Lok™ Tip, Becton, Dickenson, and Company) and placed in a KD Scientific syringe pump (model 100) to dispense the solutions at a constant rate. A high voltage power supply (Spellman CZE1000R, Spellman High Voltage Electronics Corporation) was used to apply a voltage to a blunt needle tip. Electrospinning parameters were optimized for each solution (Table 1) in order to generate continuous non-woven composite nanofibers. Randomly oriented fibers were collected onto a rotating, grounded, flat, stainless steel rectangular mandrel (7.5 x 2.5 x 0.5 cm). Scaffolds were removed from the mandrel after electrospinning and dried in the hood for 30 minutes. Using a dermal biopsy punch (AcuPunch®, Acuderm inc.), 10 mm discs were punched and used for all biomimetic mineralization experiments.

Table 1: Electrospinning parameters.

Composition (PDO:nHA:Fg)	Dispense Rate (ml/hr)	Air Gap Distance (cm)	Voltage (kV)	Needle Gauge
100:0:0	3.3	20	26	16
50:25:25	2	15	29	18
50:50:0	3.3	20	26	16
50:0:50	2	13	29	18
0:0:100	2	11	30	18
0:50:50	2	11	30	18

Biomimetic Mineralization

Different types of 1x simulated body fluids (conventional-c, revised-r, ionic-i, and modified-m) were prepared by following a published protocol [48]. Eight 10mm

(diameter) discs were punched from each of the electrospun scaffold compositions and separately incubated in 2 mL of 1x c, r, i, or m-SBF for 5 and 14 days at 37°C and 5% CO_2 atmosphere. SBF solutions were freshly prepared and replenished every 5 days. These experiments were performed under static conditions in standard tissue culture grade 24-well plates (Costar®, Corning Incorporated).

At the end of the experiment, scaffolds were removed and rinsed with DI water to wash off any minerals that were not bound to the scaffold. To visually inspect surface mineralization, one scaffold disc was dehydrated and used for SEM analysis. For mineral quantification, three scaffolds were used for alizarin red S staining and the remaining four scaffolds were analyzed using the burn-out test to calculate the percent mineral composition of the scaffolds.

Scaffold Characterization

Scanning electron microscopy (SEM) was performed in order to evaluate the scaffold and fiber surface characteristics prior to and following mineralization. Samples of electrospun scaffolds for SEM were dehydrated, mounted on aluminum stubs, sputter coated in gold (Electron Microscope Sciences model 550), and examined using a Zeiss EVO 50 XVP scanning electron microscope.

Alizarin Red S Staining

Alizarin red S (ARS) is a dye that selectively binds to calcium salts. ARS staining was used to quantify mineralization by modifying a published protocol [53]. Scaffolds

were fixed in 1 mL of formaldehyde for 10 minutes then stained with 1 mL of 40 mM alizarin red (pH adjusted to 4.1) for 30 minutes. All scaffolds were rinsed repeatedly in the well plates with DI water until all unbound dye was washed off (wash solution became clear and lost its red/pink tint). Scaffolds were then transferred into separate 2 mL tubes containing 1.5 mL of 50% acetic acid. Scaffolds were left in acetic acid overnight to ensure that all of the bound dye was dissolved. The following day 500 µL of the solubilized stain was pipetted into a 1.5 mL tube containing 600 µL of 1M NaOH in order to adjust the pH to 4.1. 200 µL of this solution was then transferred to a 96-well plate and absorbance measured at 550 nm using a SpectraMax® Plus 384 Microplate Spectrophotometer (Molecular Devices).

Burn-out Test

The mineral content in the scaffolds was also quantified by modifying a published burn-out test protocol [54]. Duration of burning was optimized for each scaffold type to ensure that all of the organic components were burned off leaving only the electrospun nHA and newly deposited minerals.

To determine burning times, the original non-mineralized scaffolds were burned at 500˚C in a platinum crucible (Engelhard-Clal, item 201-20CC) until the scaffold was completely disintegrated. Original electrospun scaffolds that did not contain nHA were burned until nothing remained in the crucible. Scaffolds containing nHA were burned until only the dry inorganic nHA powder remained in the crucible. By weighing the remaining nHA powder in the crucible after burning we are able to mathematically determine the

efficiency of incorporating hydroxyapatite into electrospun scaffolds as well as determine how much hydroxyapatite is lost during the electrospinning process. The required burn times for each scaffold type were recorded (Table 2) and applied to the same scaffold composition after mineralization.

Table 2: Duration of burn-out test for each scaffold.

Time (hours)	Scaffold Composition
1	100:0:0, 50:50:0
2	50:25:25, 0:0:100, 0:50:50
3	50:0:50

After incubation, scaffolds were rinsed, air dried for 24 hours, and then placed in a crucible of a known weight. Scaffolds were weighed (W_1), then inserted into a muffle furnace (KH Huppert Co., Type ST, Style 2A) at 500˚C for the desired time (Figure 4). A voltage rheostat (The Superior Electric Co., Powerstat, Type 116) was used as a voltage divider to keep the furnace at 500˚C throughout burning. Remaining mineral in crucible after burning was weighed (W_2) and (W_2/W_1)*100 was used to determine the percent mineral composition of the 3D scaffolds before and after mineralization. All weights were measured using a Christian Becker Analytical Balance scale (Style AB-4) accurate to 0.0001 grams.

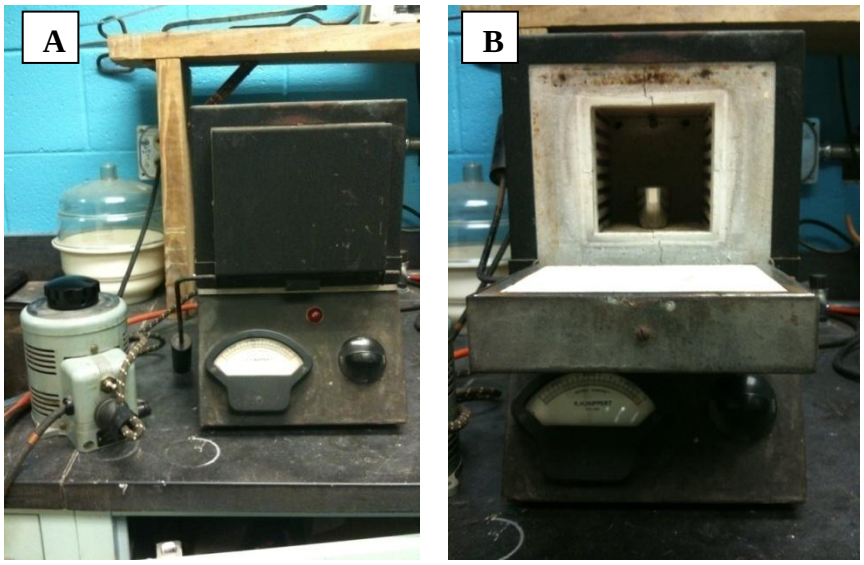

Figure 4: (A) Burn-out test setup. Muffle furnace set to 500˚C and (B) platinum crucible placed in the middle and door closed for the desired time.

Control experiments were conducted in order to verify that the hydroxyapatite was not burned off though the burn-out test. For the first control experiment, 0.2 grams of the original powdered nHA was placed in the crucible and burned for three hours. In the second experiment 0.25 grams of powder nHA was sonicated in 5 mL of HFP. After sonication the solution was left uncapped under the hood for 24 hours for the HFP to evaporate leaving only the dry sonicated nHA. This nHA was scraped off into the crucible and also burned for three hours. A burning duration of three hours was chosen because this is the maximum burn time that the scaffolds will be subjected to. After three hours in the muffle furnace, we should observe no loss or gain in weight to either of the hydroxyapatite samples. By performing these control experiments, we can prove that there is no change in weight for both powdered and sonicated nHA when sintered at 500˚C for three hours. This

also confirms that any inorganic components left in the crucible after burning the original scaffolds are attributed to the incorporated electrospun nHA.

Statistical Analysis

Statistical analysis was performed using JMP IN 4 statistical software (SAS Institute) to determine significant differences between the ARS absorbance values of different SBFs for the same scaffold composition. Analysis of the data was based on a Kruskal-Wallis one-way analysis of variance on ranks and a Tukey-Kramer pairwise multiple comparison procedure (α=0.05). The results are presented in mean ± SE.

No statistics were performed on the burn-out test results since all scaffold discs were burned and weighed once as a group of four in order to obtain a measurable amount of mineral. Once repeat experiments are conducted, statistics can be performed on the means of the groups to determine any significant differences.

CHAPTER 4 Results and Discussion

Scanning Electron Microscopy

All representative SEM images of PDO:nHA:Fg original electrospun scaffolds and scaffolds incubated in 1x c, r, i, and m-SBF for 5 and 14 days are found in Appendix A. Scaffolds without Fg (100:0:0 and 50:50:0) generally mineralized along individual fibers while scaffolds containing PDO and Fg (50:25:25 and 50:0:50) showed thin sheet-like mineral deposition throughout the scaffolds. Fibrinogen scaffolds without PDO (0:100:0 and 0:50:50) were entirely mineralized with a thick BLM layer. With the exception of 100:0:0, the pattern of mineral deposition induced by each scaffold type was consistent throughout SBFs. Figure 5 is an example which shows the general mineralization characteristics of each scaffold type in a particular SBF.

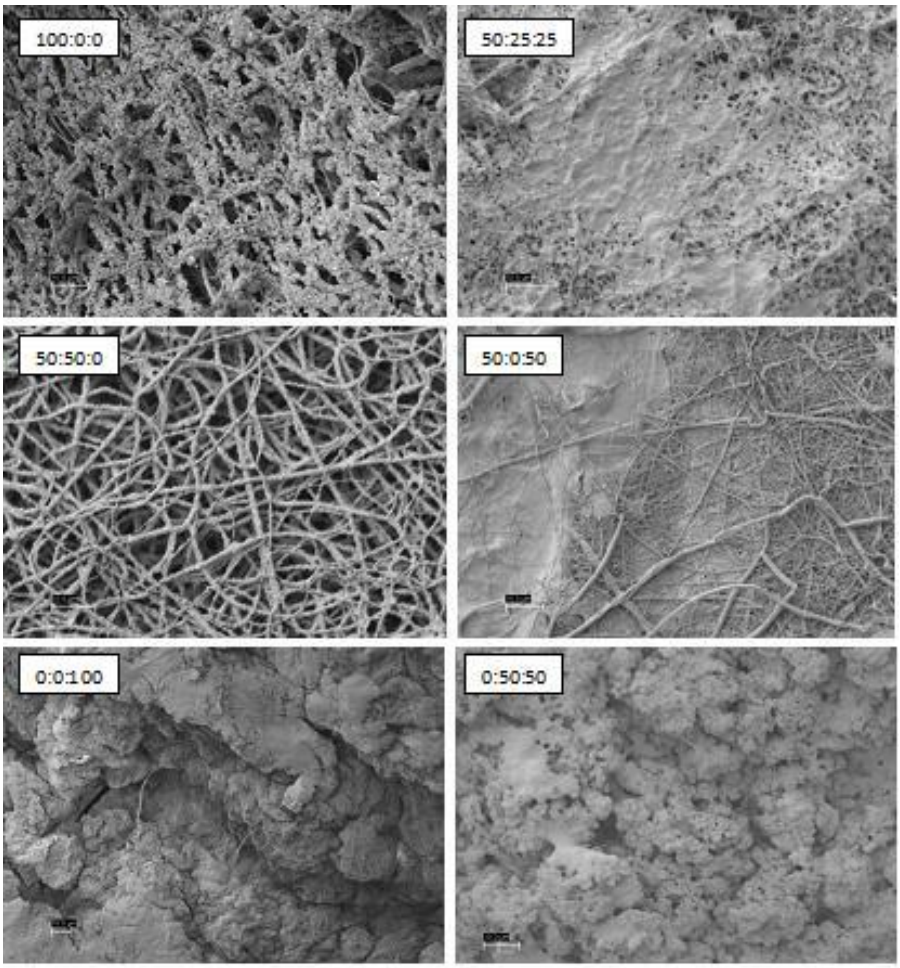

Figure 5: SEM analysis. Representative SEM images of PDO:nHA:Fg scaffolds incubated in 1x r-SBF for 14 days. Scale bars at 10µm.

A scaffold composition of 100:0:0 incubated for 14 days in different SBFs exhibited different mineralization characteristics. When immersed in c-SBF, 100:0:0 scaffolds began to degrade and lose their continuous nanofibrous structure. In r-SBF mineralization occurred on individual fibers in a bead-like formation. In i-SBF a thin layer of minerals began to grow on the outer layer of fibers however, this effect was more prominent in m-SBF (Figure 6).

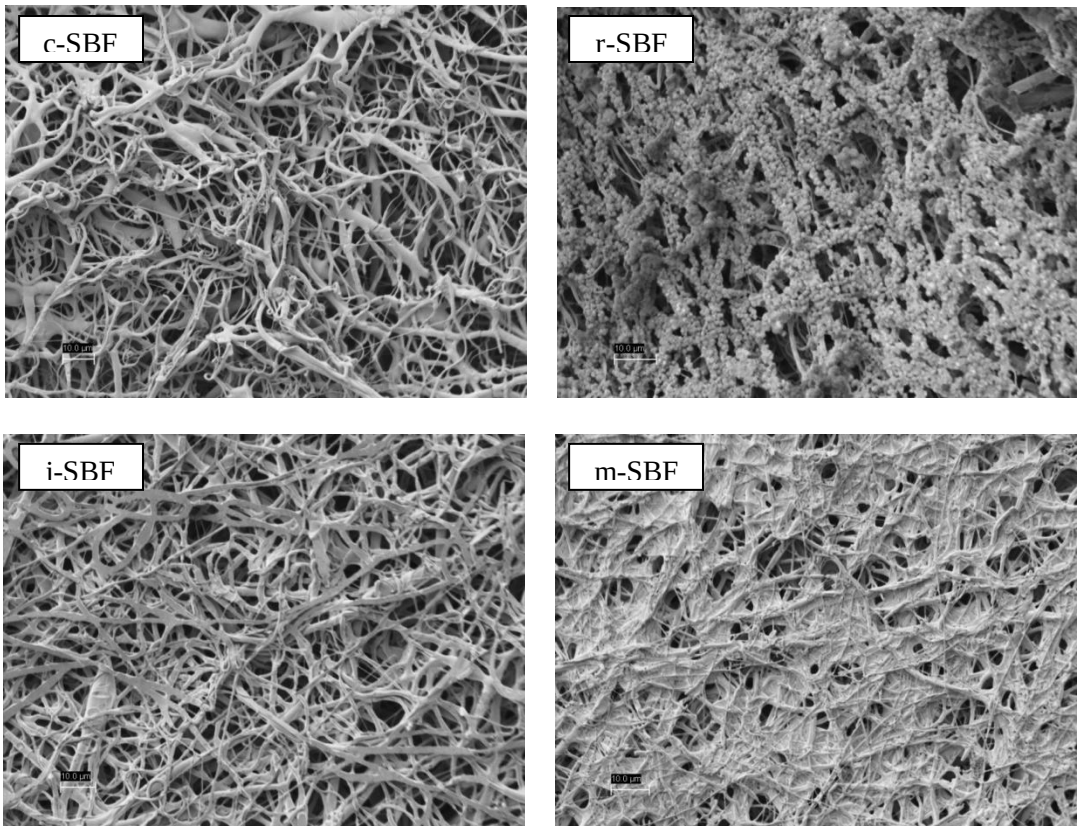

Figure 6: Mineralization patterns of 100:0:0 scaffolds in SBF for 14 days. Scale bars at 10µm.

By visual inspection of Figure 5, it seems that a composition of 100:0:0 exhibited a higher degree of mineralization compared to 50:50:0 because of the numerous mineral beads on the fibers. The only difference between these scaffolds is the addition of nHA when electrospinning. Mineral quantification of scaffolds is described later, but it is important to note that without nHA 100:0:0 scaffolds have fewer nucleation sites. As previously mentioned, primary nucleation of Ca-P occurs at nucleation sites. 100:0:0 scaffolds may have nucleation sites that are more distant from each other since it is a pure

polymer. This would cause continuous mineral growth at sparse sites where each grows on itself forming a bead-like structure at each site. Scaffolds containing nHA (50:50:0) have more nucleation sites and beads of mineral do not form. These scaffolds induce a more uniform dense individual fiber mineralization.

Overall visual progression of mineralization is observed when increasing incubation period from 5 to 14 days. Fibrinogen scaffolds not containing PDO were entirely mineralized even after 5 days suggesting 5 days immersion in 1x SBF is sufficient to grow a thick BLM layer on the scaffolds.

The SEM images show the patterns of mineralization for each scaffold type and SBF solution. Mineralization patterns varied from beads, individual fiber mineralization, thin sheets of mineral, and dense completely mineralized scaffolds. It is debated as to which mineralization pattern is preferred. Most studies have focused on mineralizing scaffolds while maintaining porosity rather than creating a dense BLM layer on the surface of the scaffold. It is believed that the best environment for increasing osteoconductivity, increasing modulus, and enhancing resistance to cellular contractile forces during tissue development exists in a mineralized porous scaffold [8, 21, 25, 33] . For the purpose of this study, the author is interested in mineralizing the scaffolds while maintaining some degree of porosity.

Scanning electron microscopy does not have the capability of determining the composition of the BLM formed on the scaffolds. X-Ray diffraction must be performed to determine this. As previously mentioned, the beginning stages of mineralization involve the nucleation of Ca-P. This primary nucleation process applies more to the scaffolds that

do not contain nHA when electrospinning. Scaffolds that initially were composed of nHA may have undergone a different mineralization process. The incorporated nHA added different nucleation sites and the BLM that was formed may have different compositions of calcium phosphates than scaffolds without electrospun nHA. Various forms of calcium phosphate based minerals can include amorphous Ca-P, octacalcium phosphate, dicalcium phosphate dehydrate, and carbonated hydroxyapatite [8, 26, 31, 33]. Again, x-ray diffraction must be performed to determine the composition of the BLM layer formed to better understand the phase and progression of mineralization on the different composition of PDO:nHA:Fg scaffolds.

Alizarin Red S Staining

Fibrinogen scaffolds without PDO (0:0:100 and 0:50:50) were not analyzed for mineral content via ARS. Scaffolds degraded after 5 days incubation in SBFs and could not be salvaged for staining. Future experiments can focus on stabilizing the mechanical integrity of these scaffolds while maintaining bioactivity.

Figure 7 graphically shows the absorbance values of the original non-mineralized electrospun scaffolds as well as the mineralized scaffolds. Original scaffolds containing nHA consistently had a higher absorbance value than mineralized scaffolds. Logic would propose that if the scaffolds are mineralized they would have a higher value than the non-mineralized scaffolds. When scaffolds are mineralized it is possible for different apatites to form (carbonated apatite, Ca-P, hydroxyapatites, etc.). No statistics were performed on this data because it is important to note that the original non-mineralized scaffolds either

contained no nHA or pure nHA. ARS may have a different binding affinity to these various apatite structures.

The environment in which the scaffolds were incubated is also an important consideration, specifically the 5% CO_2. An increase in the CO_2 concentration of the SBF will lower the pH of the mineralizing solution. HA becomes more soluble at a lower pH [55] suggesting that HA may go into solution ultimately demineralizing the scaffold resulting in a lower absorbance value.

The binding affinity of ARS to various apatites and the solubility of HA are both possible explanations for the lower absorbance values of mineralized scaffolds. Therefore, no statistics were performed to compare the original and mineralized scaffolds.

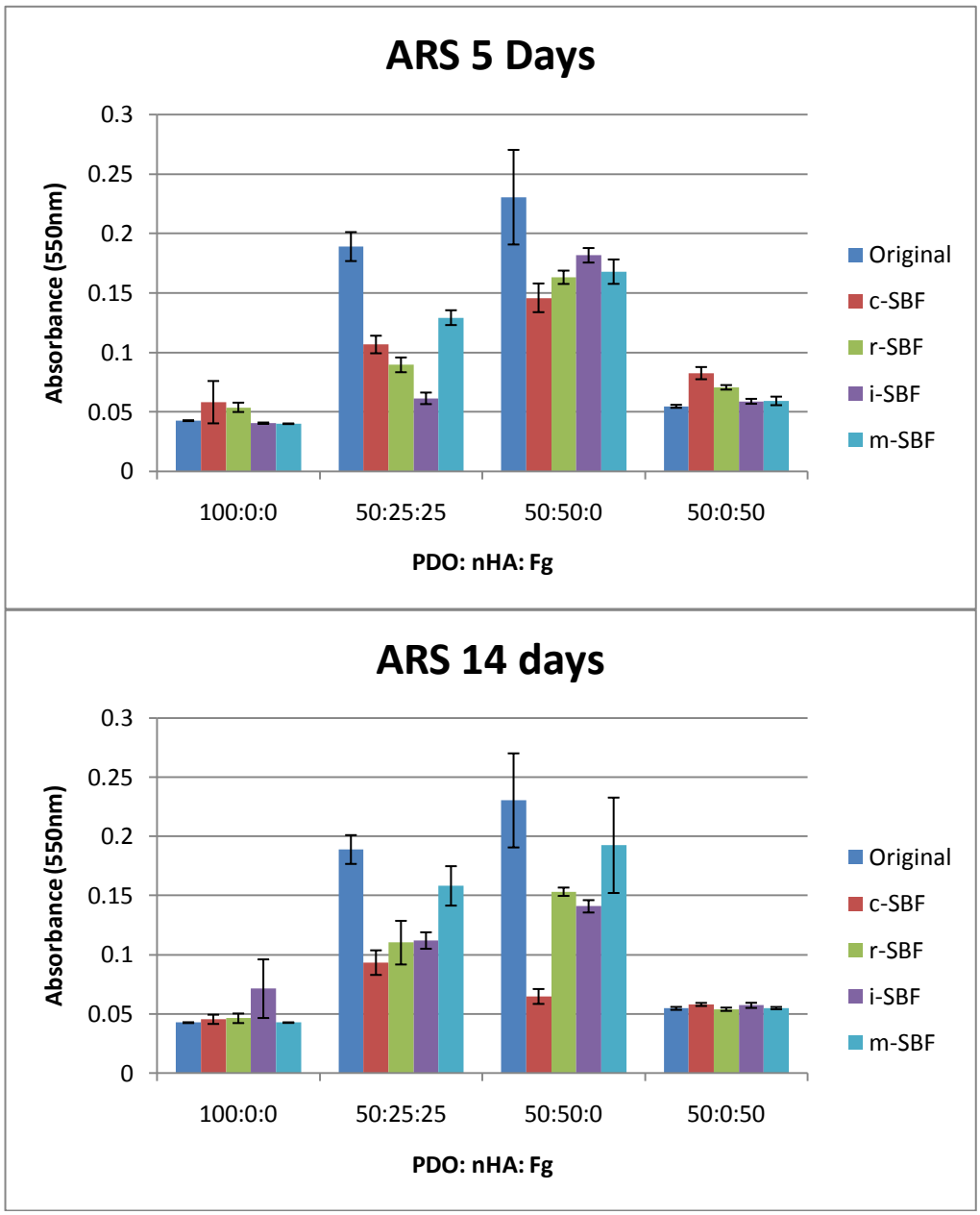

Figure 7: ARS data of original (non-mineralized) and mineralized scaffolds.

It is evident from SEMs that each scaffold mineralizes differently. Incorporation of nHA within the scaffolds could be the cause of this by initiating the nucleation of different minerals. Scaffolds without nHA most likely attract Ca-P apatites during primary

nucleation since these are the beginning steps to forming bone. Scaffolds containing nHA may attract different apatites to their surface since nHA is a higher form of Ca-P. Considering the above possibilities, statistics were performed to determine differences of SBF treatment on each scaffold type.

Figure 8 shows the absorbance values of the mineralized scaffolds and the effect of different SBFs on each scaffold composition. The control value for a scaffold with no HA was 0.0426. After 5 days incubation, the absorbance values of 100:0:0 scaffolds in all SBFs were not significantly different ($p<0.05$) from each other. An average low value of 0.0481 suggests that 100:0:0 scaffolds induced little to no mineralization independent of SBF type. Incubating 50:25:25 scaffolds in m-SBF resulted in the second highest absorbance value (0.129) and was significantly different ($p<0.05$) from r and i-SBF. This suggests that m-SBF induced more mineralization than r or i-SBF but was not statistically different ($p<0.05$) from c-SBF. Immersing 50:50:0 scaffolds in i-SBF showed the highest absorbance reading (0.182) and was significantly different ($p<0.05$) from c and r-SBF. This suggests that i-SBF is superior to c and r-SBF in mineralization potential for these scaffolds but not statistically significant ($p<0.05$) from m-SBF. The highest absorbance value for 50:0:50 scaffolds was observed in c-SBF (0.083). c-SBF was significantly different ($p<0.05$) from i and m-SBF but not from r-SBF. This implies that c-SBF mineralized 50:0:50 scaffolds better than i and m-SBFs, but not r-SBF.

The same statistical analysis of ARS data was performed on scaffolds incubated in SBF for 14 days. Absorbance readings for 100:0:0 scaffolds in different SBFs were not significantly different from each other. An average low value of 0.051 suggests that even

after 14 days 100:0:0 scaffolds induced little to no mineralization. For 50:25:25 scaffolds m-SBF had the highest value (0.158) and was only significantly different ($p<0.05$) from c-SBF. This implies that m-SBF induced more mineralization than c-SBF but was not statistically different ($p<0.05$) from r and i-SBFs. Incubating 50:50:0 scaffolds in m-SBF resulted in the highest absorbance value (0.193) which was significantly different ($p<0.05$) from all SBFs. There was no difference between SBFs for 50:0:50 scaffolds. With an average value of 0.056, little to no mineralization occurred.

The same statistical analysis was used to compare scaffolds compositions for 5 and 14 days incubation in SBF. 100:0:0 scaffolds showed statistical difference between day 5 and 14. For 50:25:25 scaffolds, 5 days in m-SBF was only significantly different ($p<0.05$) than 5 days in i-SBF while 14 days in m-SBF was significantly different ($p<0.05$) than 5 days in r and i-SBF and 14 days in c-SBF. This data does not concretely prove that one SBF performs better than the other when comparing day 5 and 14 in 50:25:25 scaffolds. Statistical analysis performed on 50:50:0 scaffolds resulted in the same conclusion. Howerever, 50:0:50 scaffolds incubated in c-SBF for 5 days was statistically significant ($p<0.005$) to all of the SBFs except i-SBF for 5 days. This suggests that 50:0:50 scaffolds in either c or i-SBF for 5 days induce more mineralization than scaffolds incubated in any other SBF for 5 or 14 days.

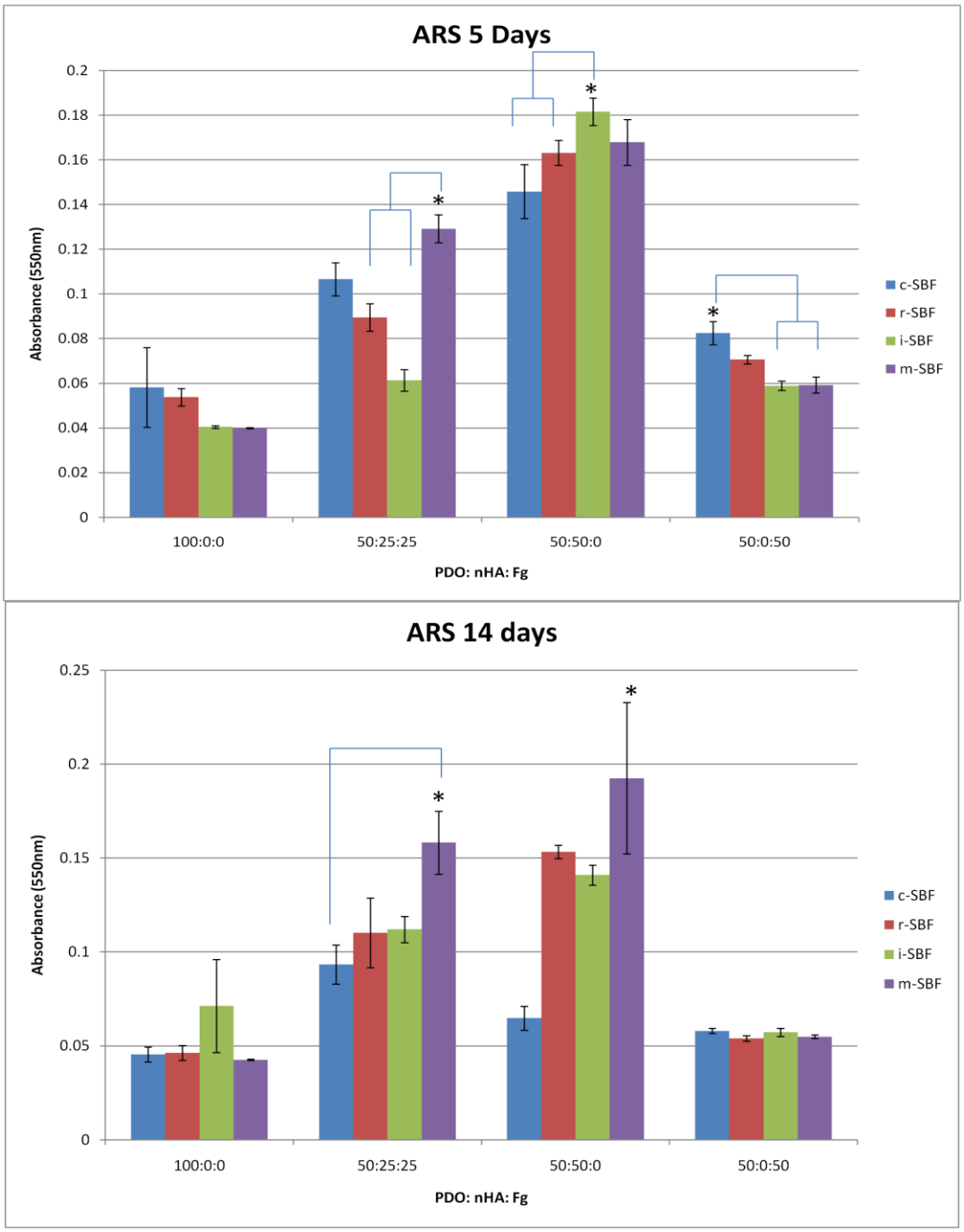

Figure 8: ARS data and statistics for mineralized scaffolds. * denotes statistical significance ($p<0.05$).

For both 5 and 14 days, higher absorbance readings were recorded for 50:50:0 scaffolds showing a visible pattern of increased absorbance values with increased nHA composition. The ARS data suggests that 5 days incubation of 50:50:0 in SBFs is sufficient to induce mineralization while the other scaffold compositions showed no noticiable difference between 5 and 14 days. The addition of Fg did not have an effect on the ARS results when mineralizing scaffolds. Considering the concerns regarding different apatite formation and pH effects, ARS may not be the most accurate method of quantifying mineral present within the scaffold. This data can be analyzed more effectively if the composition of the mineral formed was known.

Burn-Out Test

As previously mentioned, 0:0:100 and 0:50:50 scaffolds degraded after 5 days incubation in SBFs and were not salvaged for mineral quantification via burn-out test. The remaining scaffolds were intact and analyzed.

Figure 9 shows that upon burning the scaffolds (before or after mineralization), the organic components (polymeric nanofibers) are entirely burned off leaving only the inorganic mineral. These control experiments validate that the burn-out test is an effective method to quantify the scaffold mineral content. Figure 9 shows images of scaffolds in the crucible before and after burning to provide a macroscopic view of the leftover mineral contents. As predicted, scaffolds which contained nHA had more visible leftover mineral in the scaffold after burning.

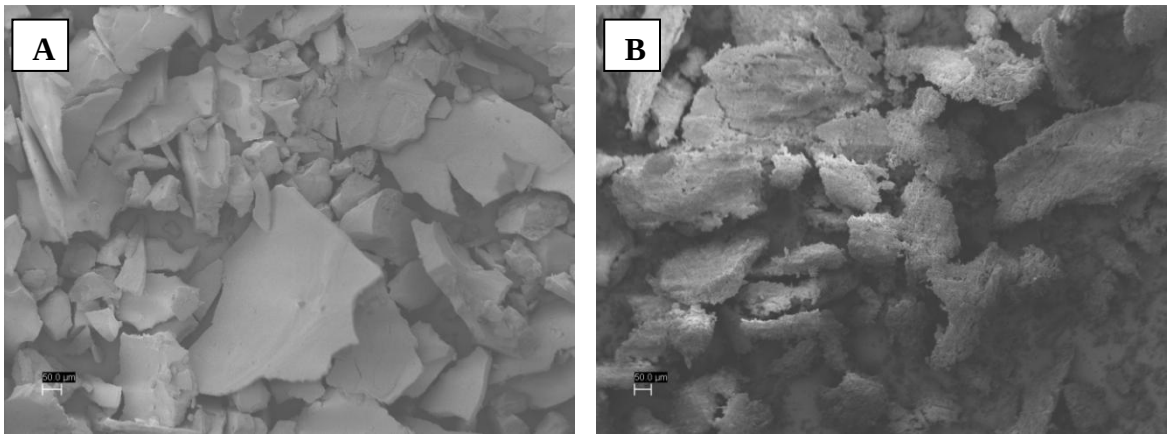

Figure 9: SEM of remaining mineral after burn-out test. (A) 50:50:0 not treated with SBF and (B) 50:25:25 treated with r-SBF for 14 days. These are not individual nanocrystals, but rather a cluster of minerals that were scrapped from the crucible. Scale bars at 50µm.

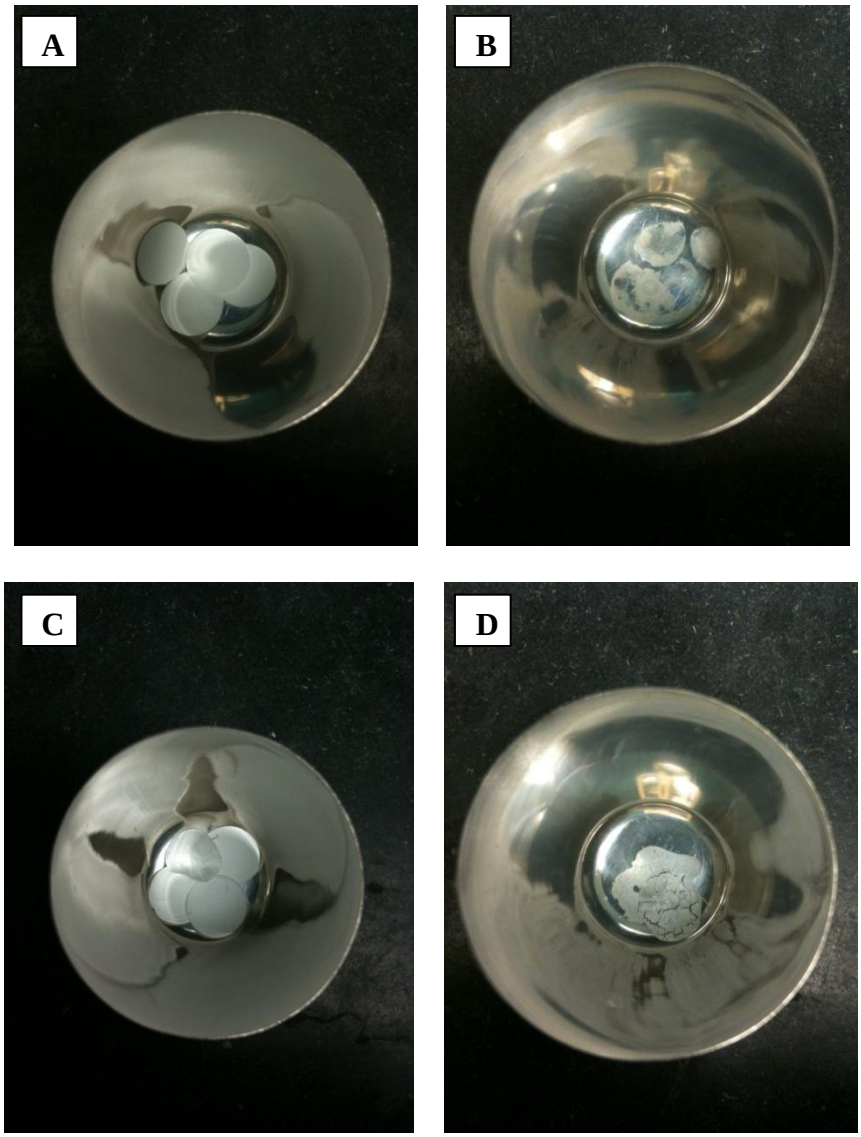

Figure 10: Mineralized scaffolds before and after burn-out test. 100:0:0 scaffolds incubated for 5 days in m-SBF (A) before and (B) after burn. 50:50:0 scaffolds incubated for 5 days in i-SBF (C) before and (D) after burn-out test.

Percent mineral composition of the scaffolds was calculated by weighing scaffolds before and after burning. All PDO:nHA:Fg scaffold compositions were analyzed for mineral content before and after incubation in different SBFs for 5 and 14 days under static conditions (Figure 11). Again, no statistics were performed on the burn-out test data since

only one trial was conducted. However, observations can still be extracted from the presented data.

The percent mineral composition of the original electrospun scaffolds prior to mineralization served as the control. It also provided a method to measure the effectiveness of incorporating nHA within electrospun scaffolds by determining how much nHA was actually incorporated and how much was lost during the electrospinning process. Polymer solutions that were prepared without nHA (100:0:0 and 50:0:50) yielded a value of 0% mineral. This control verifies that all the PDO and Fg are completely burned off. Solutions containing 25% (50:25:25) and 50% nHA (50:50:0) yielded values of 16.3% and 41.7% respectively. This suggests that 34.8% and 16.6% nHA was lost respectively during the electrospinning process. The 50:25:25 composite scaffolds may have lost more nHA during electrospinning because these solutions contained Fg while the 50:50:0 did not. Additional experiments can be designed to study the effect of Fg on incorporating nHA in electrospun scaffolds. As far as these results are concerned, a scaffold composition of 50:50:0 resulted in the highest percent yield of nHA incorporated at 83.4%.

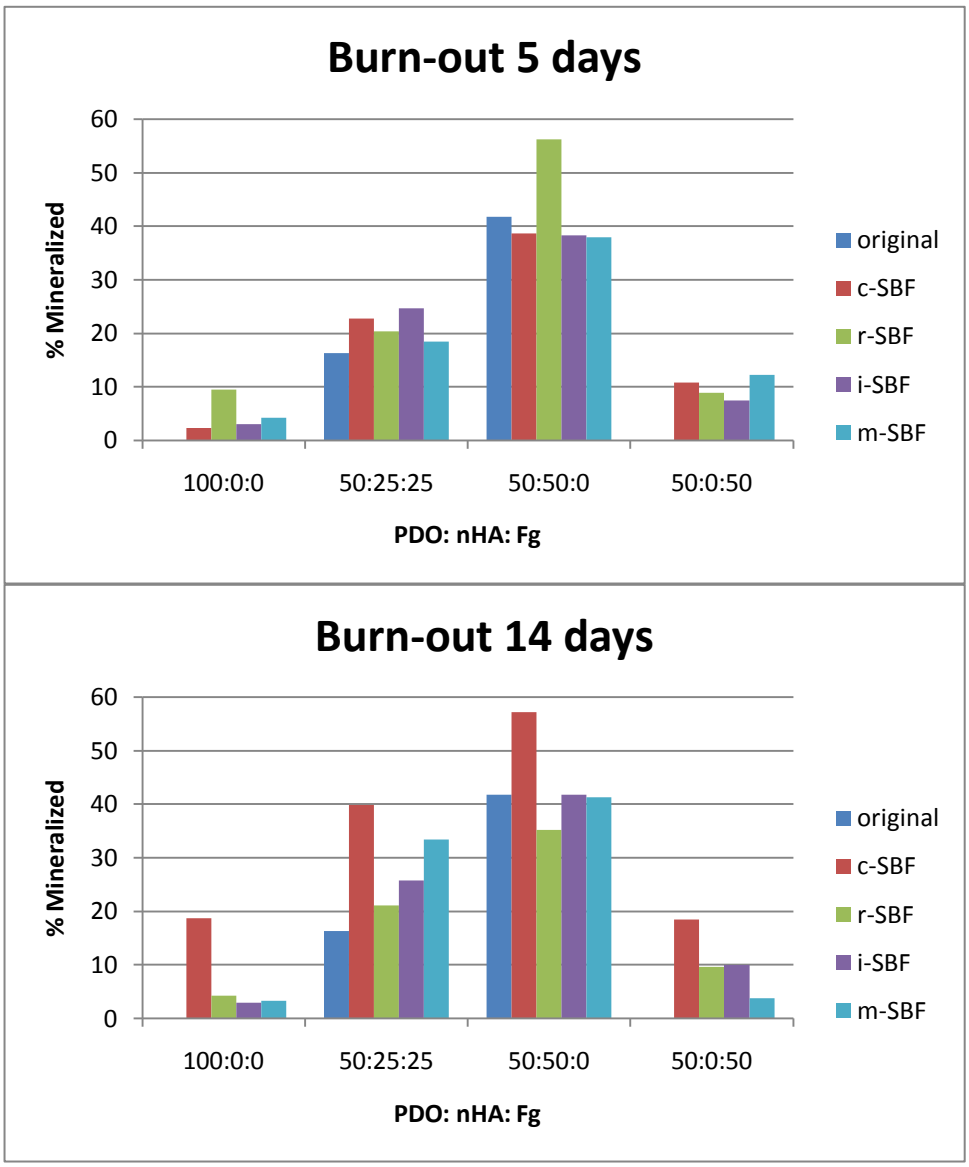

Figure 11: Burn-out test data. Graphs represent the percent mineral composition of original and mineralized PDO:nHA:Fg scaffolds in different SBFs for 5 and 14 days.

After 5 days incubation in different SBFs, PDO:nHA:Fg scaffolds were burned to quantify mineral content. All 100:0:0 scaffolds mineralized to some degree compared to original scaffold mineral composition of 0%. Scaffolds incubated in c, i, and m-SBFs each were comprised of approximately 3% mineral. Scaffolds incubated in r-SBF had a mineral

composition of 9.6%. All 50:25:25 scaffolds increased in mineral content when compared to the original mineral composition (16%). Scaffolds in c, r, i, and m-SBF contained 22.8%, 20.4%, 24.7%, and 18.4% respectively. 50:50:0 scaffolds incubated in c, i, and m-SBFs resulted in a slightly lower mineral composition (38%) when compared to the original (41.7%). The highest percent mineral content was observed in 50:50:0 scaffolds in r-SBF (56.2%). 50:0:50 scaffolds incubated in all SBFs increased in mineral content from 0% to about 10%. Overall the largest percent increase was noticed in 50:50:0 scaffolds in r-SBF for 5 days. These scaffolds in r-SBF also showed the highest percent mineral composition. By comparing scaffold compositions, it is evident that 50:50:0 scaffolds contained the highest mineral content before and after mineralization. This was expected since more nHA was incorporated within these scaffolds during the electrospinning process.

For each scaffold composition, incubation in c-SBF for 14 days resulted in the highest percent mineral content and highest mineral increase due to SBF treatment suggesting that c-SBF induces the most mineralization independent of scaffold composition. After 14 days, 100:0:0 scaffolds in c-SBF increased in mineral content from 0% to 18.6%. All other SBFs only resulted in about 3% mineral content. All mineralized 50:25:25 scaffolds increased in mineral content from 16.3% to 39.8% (c-SBF), 21.1% (r-SBF), 25.7% (i-SBF), and 33.3% (m-SBF). 50:50:0 scaffolds incubated in i and m-SBF had no effect on mineral content (41%). Incubation in c and i-SBF resulted in 57.1% and 29.1% mineral composition, respectively. The difference between c and i-SBF suggest that 50:50:0 scaffolds mineralize differently depending on SBF. After 14 days, 50:0:50

scaffolds increased in mineral content from 0% to various values depending on SBF type. 50:0:50 scaffolds incubated in c, r, i, and m-SBF resulted in 18.4%, 9.6%, 10%, and 3.7% mineral content, respectively. The difference between c and m-SBF suggest that 50:0:50 scaffolds mineralize differently depending on SBF type. Once again 50:50:0 scaffolds contained higher percentages of mineral composition before and after mineralization since nHA was originally incorporated within the scaffolds. However, the highest overall mineral increase due to SBF treatment was in 50:25:25 scaffolds incubated in c-SBF for 14 days. Percent mineral content increased from 16.3% to 39.8% suggesting that 50:25:25 scaffolds in c-SBF for 14 days induce the most mineralization.

From 5 to 14 days, some values increased while some decreased. The increases of mineral content can be attributed to the deposition of minerals on the electrospun scaffolds. The decreases may result from the solubility of nHA at a lower pH as previously described. Scaffolds without nHA (100:0:0 and 50:0:50) never surpassed 20% mineral content while 50:25:25 and 50:50:0 scaffolds reached up to 40% and 57%, respectively. 50:50:0 scaffolds in r-SBF for 5 days and 50:50:0 scaffolds in c-SBF for 14 days contained similar percent mineral compositions (~57%). Since 50:50:0 scaffolds in r-SBF for 5 days reached a high mineral content just after 5 days, we can assume that these scaffolds will bond to the host bone faster than the same scaffolds in c-SBF for 14 days. The data above is from one trial, statistics were not performed meaning that some higher or lower values may not be significantly different. However, the graphs do provide a general view of the effect of SBFs, which scaffold compositions have higher mineralization potentials, and the advantages of incorporating nHA.

CHAPTER 5 Conclusion

This study has demonstrated an easy, cost effective, reproducible approach using synthetic polymers, natural polymers, and inorganic apatites to produce a nanofibrous scaffold for bone tissue engineering applications. By combining electrospinning (PDO, Fg, nHA) and mineralization (SBF) methods, scaffolds with mineralized nanofibers were produced. Also, a reliable method for quantifying mineral content of 3D porous scaffolds before and after mineralization was developed. The degree and type of mineralization was dependent on the scaffold composition, type of SBF, and duration of incubation.

The addition of Fg resulted in thin sheet-like deposition of minerals unlike individual fiber mineralization seen in PDO and PDO-nHA scaffolds. Mineralized electrospun Fg scaffolds not containing PDO were not stable, but had superior mineralization capabilities which produced a thick BLM layer throughout the scaffolds. Mineral quantification revealed that overall, 50:50:0 scaffolds had the highest mineral content.

ARS and burn-out test data did not support each regarding which SBF type has the highest potential to induce mineralization. There are many variables to consider when quantifying mineralization via ARS which make it difficult to compare the different scaffold compositions. The burn-out test is a more reliable method to quantify the mineral

content of scaffolds. These results indicated that after 14 days, c-SBF was most efficient in inducing mineralization independent of scaffold composition. 50:50:0 scaffolds incubated in r-SBF for 5 days and c-SBF for 14 days contained the highest percent mineral composition. 50:25:25 scaffolds incubated in c-SBF for 14 days showed the highest increase in mineral content suggesting that this scaffold composition has superior mineralization capabilities.

This study focused on developing a mineralized porous nanofibrous scaffold intended for cleft palate repair. Results show that Fg containing scaffolds have superior mineralization potential but tend to mineralize as sheets decreasing the porosity of the scaffold. 50:50:0 scaffolds incubated in either r-SBF for 5 days or c-SBF for 14 days produce scaffolds with high mineral content and individual mineralized fibers. These mineralized scaffolds were still porous and can potentially serve as effective substrates to induce bone formation.

Literature Cited

Literature Cited

1. Fallin, M.D., et al., *Family-based analysis of MSX1 haplotypes for association with oral clefts.* Genet Epidemiol, 2003. **25**(2): p. 168-75.
2. Zhang, Z., et al., *Rescue of cleft palate in Msx1-deficient mice by transgenic Bmp4 reveals a network of BMP and Shh signaling in the regulation of mammalian palatogenesis.* Development, 2002. **129**(17): p. 4135-46.
3. Sandy, J.R., *Molecular, clinical and political approaches to the problem of cleft lip and palate.* Surgeon, 2003. **1**(1): p. 9-16.
4. Sadove, A.M., J.A. van Aalst, and J.A. Culp, *Cleft palate repair: art and issues.* Clin Plast Surg, 2004. **31**(2): p. 231-41.
5. Moreau, J.L., et al., *Tissue engineering solutions for cleft palates.* J Oral Maxillofac Surg, 2007. **65**(12): p. 2503-11.
6. Logeart-Avramoglou, D., et al., *Engineering bone: challenges and obstacles.* J Cell Mol Med, 2005. **9**(1): p. 72-84.
7. Kim, S.S., et al., *Poly(lactide-co-glycolide)/hydroxyapatite composite scaffolds for bone tissue engineering.* Biomaterials, 2006. **27**(8): p. 1399-409.
8. Al-Munajjed, A.A., et al., *Development of a biomimetic collagen-hydroxyapatite scaffold for bone tissue engineering using a SBF immersion technique.* J Biomed Mater Res B Appl Biomater, 2009. **90**(2): p. 584-91.

9. Kim, S.S., et al., *A poly(lactide-co-glycolide)/hydroxyapatite composite scaffold with enhanced osteoconductivity.* J Biomed Mater Res A, 2007. **80**(1): p. 206-15.

10. Venugopal, J.R., et al., *Nanobioengineered electrospun composite nanofibers and osteoblasts for bone regeneration.* Artif Organs, 2008. **32**(5): p. 388-97.

11. Kim, S.S., et al., *Accelerated bonelike apatite growth on porous polymer/ceramic composite scaffolds in vitro.* Tissue Eng, 2006. **12**(10): p. 2997-3006.

12. So, L.L. and W.W. Lui, *Alternative donor site for alveolar bone grafting in adults with cleft lip and palate.* Angle Orthod, 1996. **66**(1): p. 9-16.

13. Nadal, E., et al., *Secondary Alveolar Bone Grafting: Our Experience With Olecranon Bone Graft.* J Craniofac Surg, 2010.

14. Ciardelli, G., et al., *Enzymatically crosslinked porous composite matrices for bone tissue regeneration.* J Biomed Mater Res A, 2010. **92**(1): p. 137-51.

15. Weiner, S. and W. Traub, *Bone structure: from angstroms to microns.* Faseb J, 1992. **6**(3): p. 879-85.

16. Salo, J., *Bone resorbing osteoclasts reveal two basal plasma membrane domains and transcytosis of degraded matrix material.* Anatomy and Cell Biology, 2002.

17. Jang, J.H., O. Castano, and H.W. Kim, *Electrospun materials as potential platforms for bone tissue engineering.* Adv Drug Deliv Rev, 2009. **61**(12): p. 1065-83.

18. Madurantakam, P.A., et al., *Multiple factor interactions in biomimetic mineralization of electrospun scaffolds.* Biomaterials, 2009. **30**(29): p. 5456-64.

19. Hutmacher, D.W., et al., *State of the art and future directions of scaffold-based bone engineering from a biomaterials perspective.* J Tissue Eng Regen Med, 2007. **1**(4): p. 245-60.

20. Glimcher, M.J., *Mechanism of calcification: role of collagen fibrils and collagen-phosphoprotein complexes in vitro and in vivo.* Anat Rec, 1989. **224**(2): p. 139-53.

21. Shin, K., A.C. Jayasuriya, and D.H. Kohn, *Effect of ionic activity products on the structure and composition of mineral self assembled on three-dimensional poly(lactide-co-glycolide) scaffolds.* J Biomed Mater Res A, 2007. **83**(4): p. 1076-86.

22. Langer, R. and J.P. Vacanti, *Tissue engineering.* Science, 1993. **260**(5110): p. 920-6.

23. Murugan, R. and S. Ramakrishna, *Nano-featured scaffolds for tissue engineering: a review of spinning methodologies.* Tissue Eng, 2006. **12**(3): p. 435-47.

24. Liao, S., et al., *Processing nanoengineered scaffolds through electrospinning and mineralization suitable for biomimetic bone tissue engineering.* J Mech Behav Biomed Mater, 2008. **1**(3): p. 252-60.

25. Murphy, W.L., D.H. Kohn, and D.J. Mooney, *Growth of continuous bonelike mineral within porous poly(lactide-co-glycolide) scaffolds in vitro.* J Biomed Mater Res, 2000. **50**(1): p. 50-8.

26. Oyane, A., et al., *Simple surface modification of poly(epsilon-caprolactone) to induce its apatite-forming ability.* J Biomed Mater Res A, 2005. **75**(1): p. 138-45.

27. Jayasuriya, A.C., et al., *Acceleration of biomimetic mineralization to apply in bone regeneration.* Biomed Mater, 2008. **3**(1): p. 015003.

28. Zhang, R. and P.X. Ma, *Biomimetic polymer/apatite composite scaffolds for mineralized tissue engineering.* Macromol Biosci, 2004. **4**(2): p. 100-11.

29. Zhang, D., J. Chang, and Y. Zeng, *Fabrication of fibrous poly(butylene succinate)/wollastonite/apatite composite scaffolds by electrospinning and biomimetic process.* J Mater Sci Mater Med, 2008. **19**(1): p. 443-9.

30. Prabhakaran, M.P., J. Venugopal, and S. Ramakrishna, *Electrospun nanostructured scaffolds for bone tissue engineering.* Acta Biomater, 2009. **5**(8): p. 2884-93.

31. Chen, J., B. Chu, and B.S. Hsiao, *Mineralization of hydroxyapatite in electrospun nanofibrous poly(L-lactic acid) scaffolds.* J Biomed Mater Res A, 2006. **79**(2): p. 307-17.

32. Zhang, Y.Z., et al., *Biomimetic and bioactive nanofibrous scaffolds from electrospun composite nanofibers.* Int J Nanomedicine, 2007. **2**(4): p. 623-38.

33. Li, X., et al., *Coating electrospun poly(epsilon-caprolactone) fibers with gelatin and calcium phosphate and their use as biomimetic scaffolds for bone tissue engineering.* Langmuir, 2008. **24**(24): p. 14145-50.

34. Yu, H.S., et al., *Apatite-mineralized polycaprolactone nanofibrous web as a bone tissue regeneration substrate.* J Biomed Mater Res A, 2009. **88**(3): p. 747-54.

35. Carlisle, C.R., et al., *The mechanical properties of individual, electrospun fibrinogen fibers.* Biomaterials, 2009. **30**(6): p. 1205-13.

36. Laurencin, C.T., et al., *Tissue engineering: orthopedic applications.* Annu Rev Biomed Eng, 1999. **1**: p. 19-46.

37. Hubbell, J.A., *Biomaterials in tissue engineering.* Biotechnology (N Y), 1995. **13**(6): p. 565-76.

38. Sell, S.A., et al., *Cross-linking methods of electrospun fibrinogen scaffolds for tissue engineering applications.* Biomed Mater, 2008. **3**(4): p. 045001.

39. McManus, M.C., et al., *Electrospun fibrinogen: feasibility as a tissue engineering scaffold in a rat cell culture model.* J Biomed Mater Res A, 2007. **81**(2): p. 299-309.

40. Doolittle, R.F., *Fibrinogen and fibrin.* Annu Rev Biochem, 1984. **53**: p. 195-229.

41. Erban, J.K., *P-selectin and wound healing.* Behring Inst Mitt, 1993(92): p. 248-57.

42. Weigel, P.H., G.M. Fuller, and R.D. LeBoeuf, *A model for the role of hyaluronic acid and fibrin in the early events during the inflammatory response and wound healing.* J Theor Biol, 1986. **119**(2): p. 219-34.

43. McManus, M.C., et al., *Mechanical properties of electrospun fibrinogen structures.* Acta Biomater, 2006. **2**(1): p. 19-28.

44. Fisher, J.P., et al., *Effect of biomaterial properties on bone healing in a rabbit tooth extraction socket model.* J Biomed Mater Res A, 2004. **68**(3): p. 428-38.

45. Bigi, A., et al., *Bonelike apatite growth on hydroxyapatite-gelatin sponges from simulated body fluid.* J Biomed Mater Res, 2002. **59**(4): p. 709-15.

46. Ohgushi, H. and A.I. Caplan, *Stem cell technology and bioceramics: from cell to gene engineering.* J Biomed Mater Res, 1999. **48**(6): p. 913-27.

47. Stupp, S.I. and G.W. Ciegler, *Organoapatites: materials for artificial bone. I. Synthesis and microstructure.* J Biomed Mater Res, 1992. **26**(2): p. 169-83.

48. Oyane, A., et al., *Preparation and assessment of revised simulated body fluids.* J Biomed Mater Res A, 2003. **65**(2): p. 188-95.

49. Kokubo, T., et al., *Solutions able to reproduce in vivo surface-structure changes in bioactive glass-ceramic A-W.* J Biomed Mater Res, 1990. **24**(6): p. 721-34.

50. Kokubo, T. and H. Takadama, *How useful is SBF in predicting in vivo bone bioactivity?* Biomaterials, 2006. **27**(15): p. 2907-15.

51. Zhang, R. and P.X. Ma, *Poly(alpha-hydroxyl acids)/hydroxyapatite porous composites for bone-tissue engineering. I. Preparation and morphology.* J Biomed Mater Res, 1999. **44**(4): p. 446-55.

52. Sell, S., et al., *Scaffold permeability as a means to determine fiber diameter and pore size of electrospun fibrinogen.* J Biomed Mater Res A, 2008. **85**(1): p. 115-26.

53. Gregory, C.A., et al., *An Alizarin red-based assay of mineralization by adherent cells in culture: comparison with cetylpyridinium chloride extraction.* Anal Biochem, 2004. **329**(1): p. 77-84.

54. Song, Y., S. Wen, and M. Li, *The investigation on preparation & physicochemical process of nanosized hydroxyapatite powder.* Materials Research Society, 2002. **724**: p. 135-140.

55. Elliott, J.C., *Structure and Chemistry of Apatites and other Calcium Orthophosphates.* Elsevier, 1994.

APPENDIX A

Scanning Electron Microscopy Images

In all of the following SEM images, the scale bars are 10µm.

Original Electrospun PDO:nHA:Fg Scaffolds

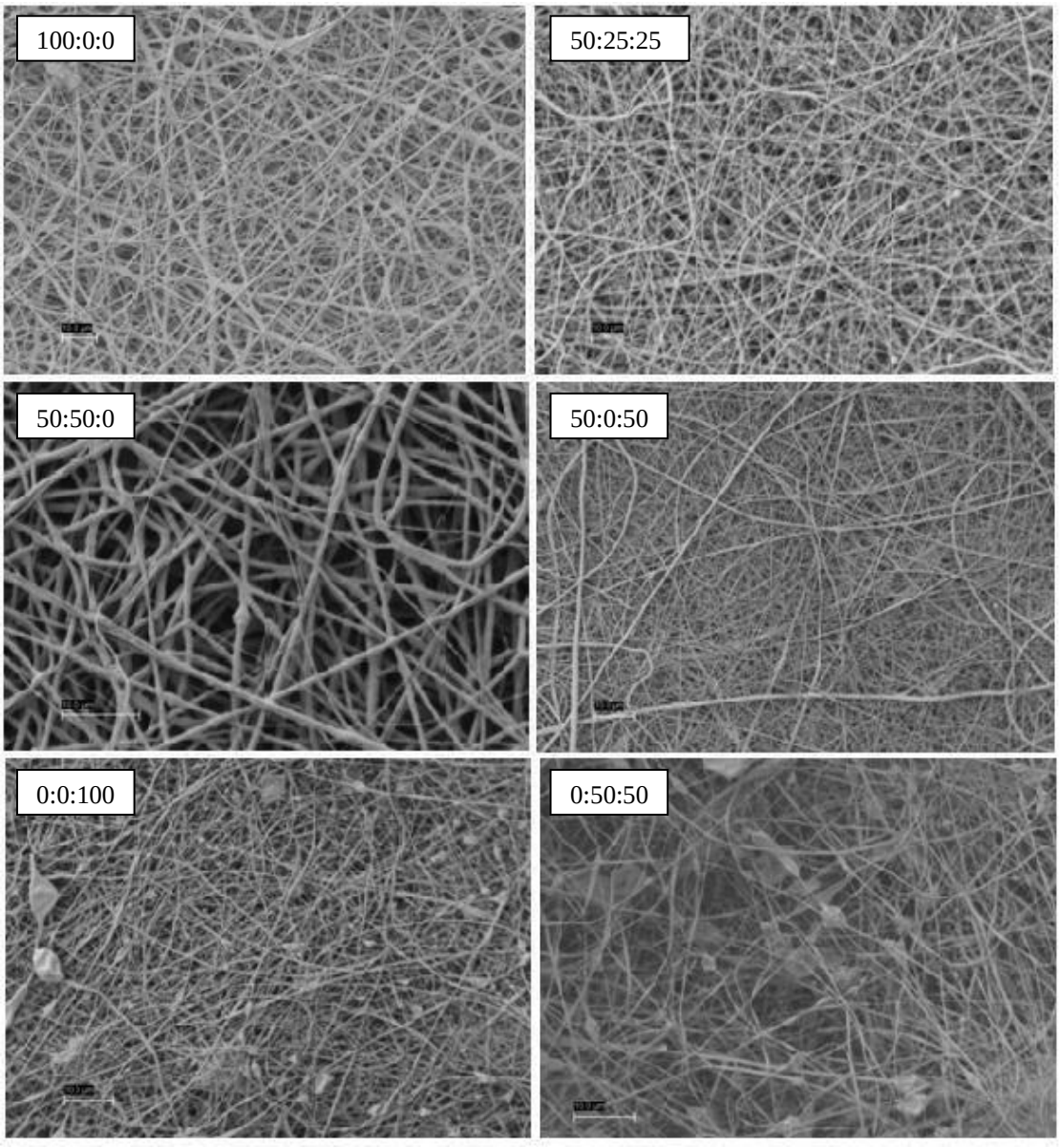

PDO:nHA:Fg Scaffolds Incubated in c-SBF for 5 days

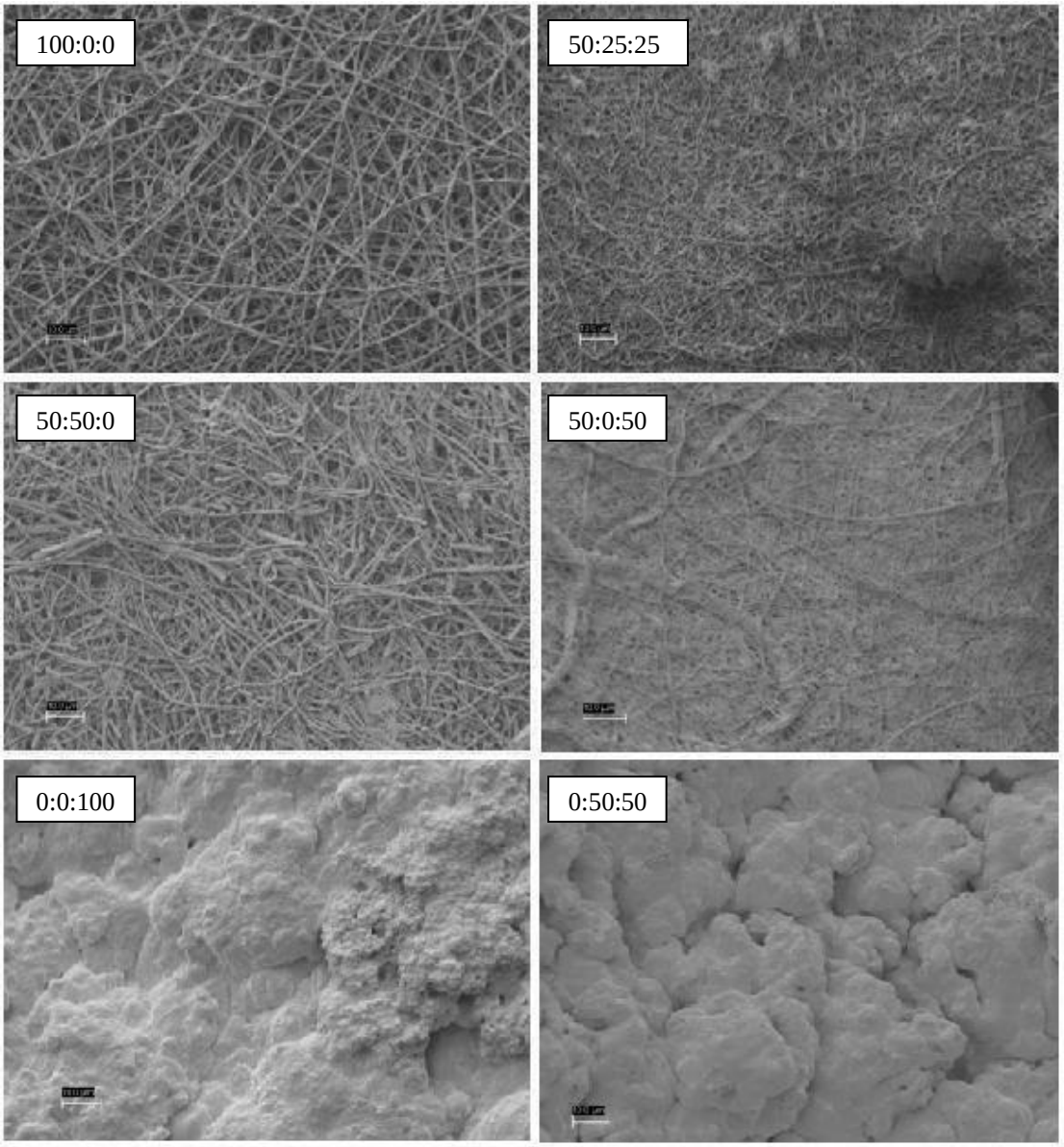

PDO:nHA:Fg Scaffolds Incubated in c-SBF for 14 days

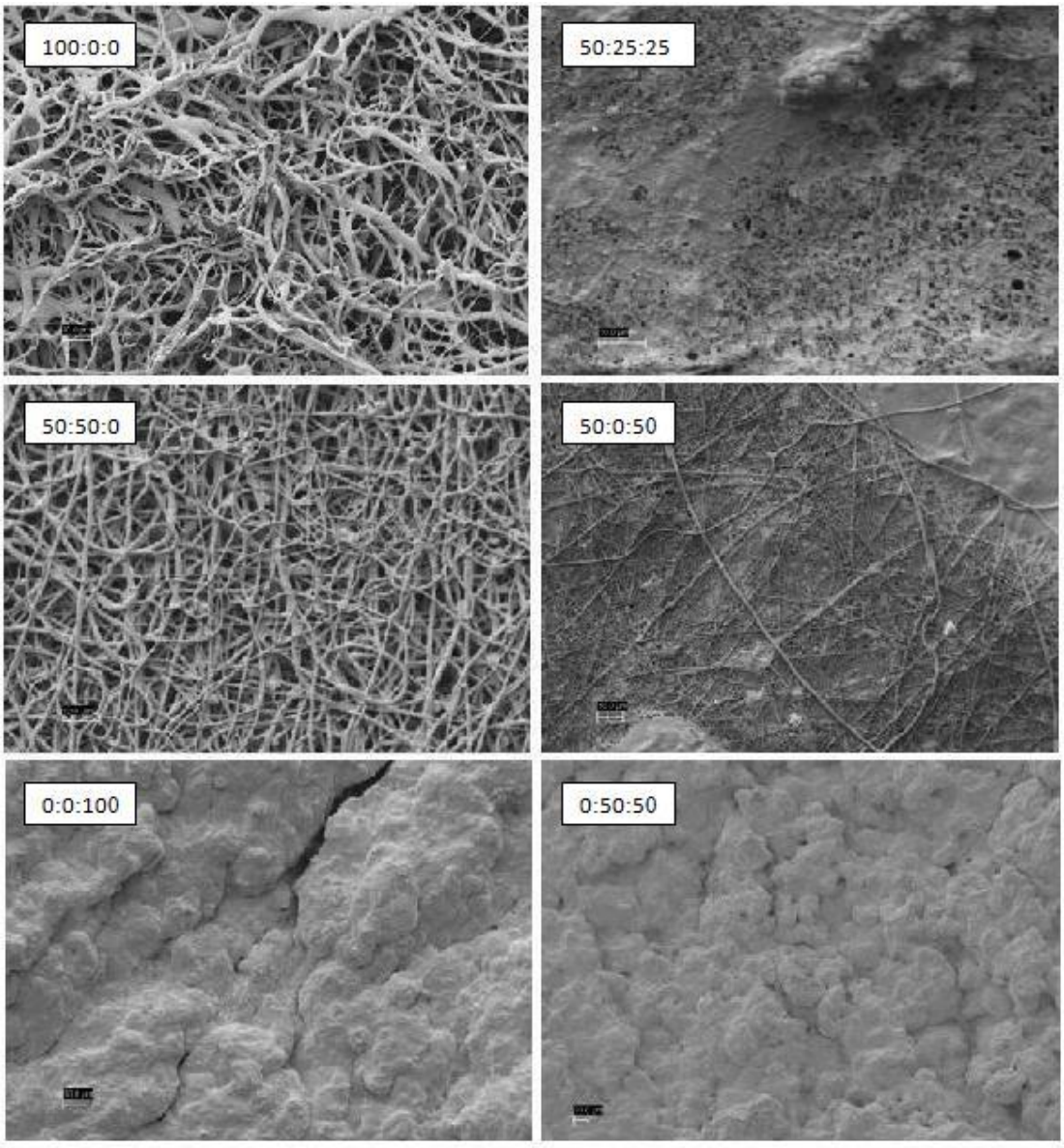

PDO:nHA:Fg Scaffolds Incubated in r-SBF for 5 days

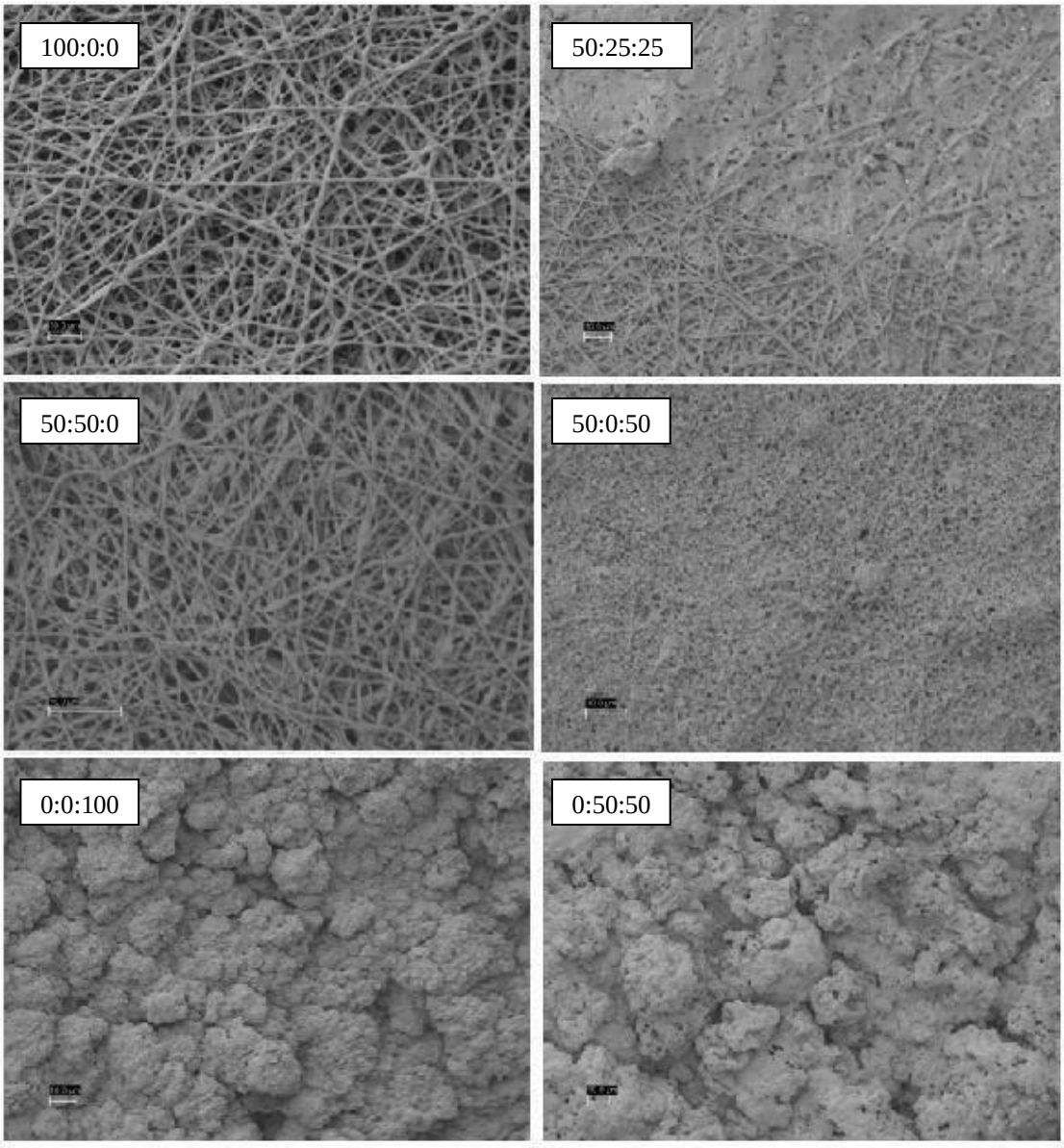

PDO:nHA:Fg Scaffolds Incubated in r-SBF for 14 days

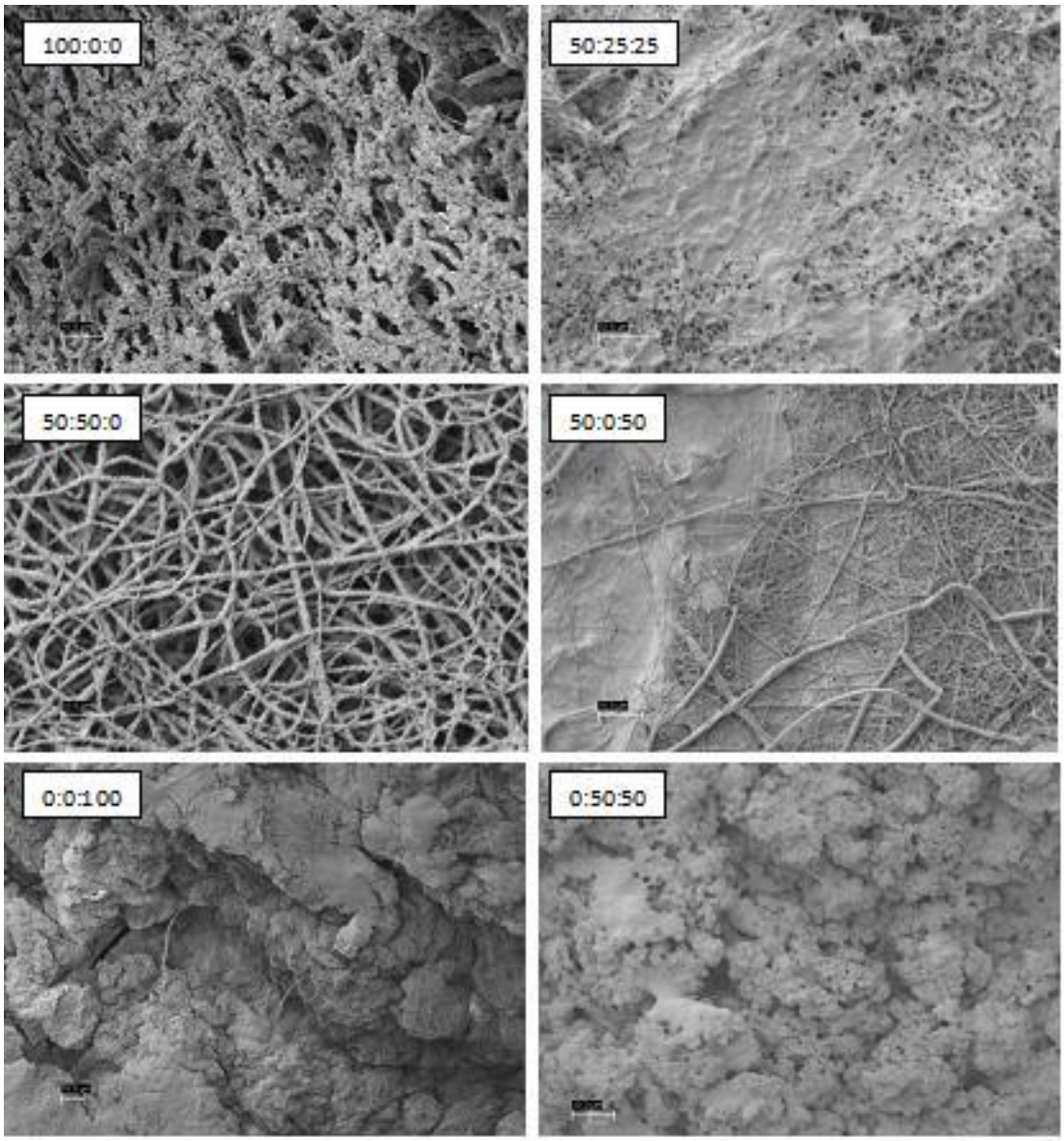

PDO:nHA:Fg Scaffolds Incubated in i-SBF for 5 days

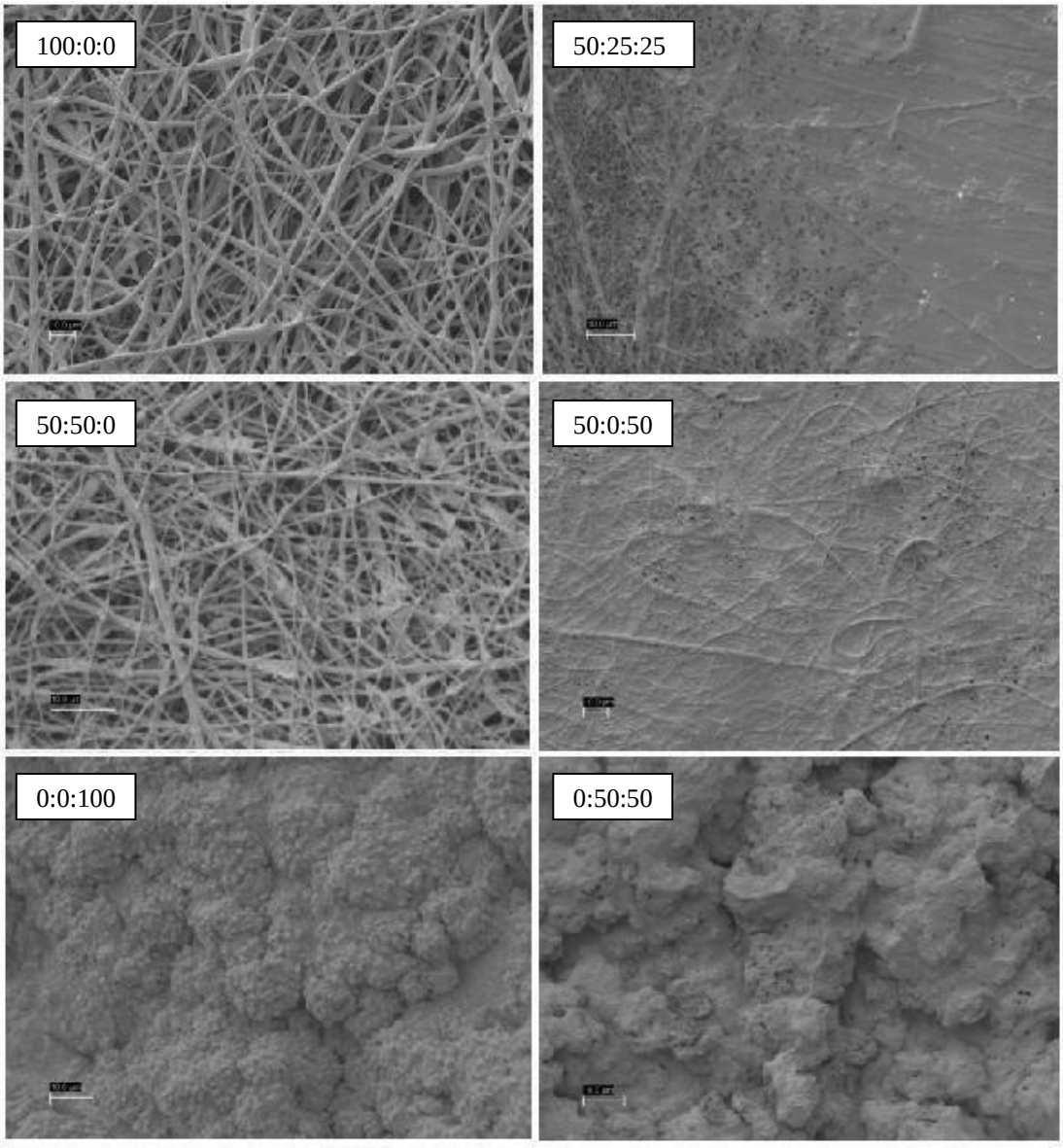

PDO:nHA:Fg Scaffolds Incubated in i-SBF for 14 days

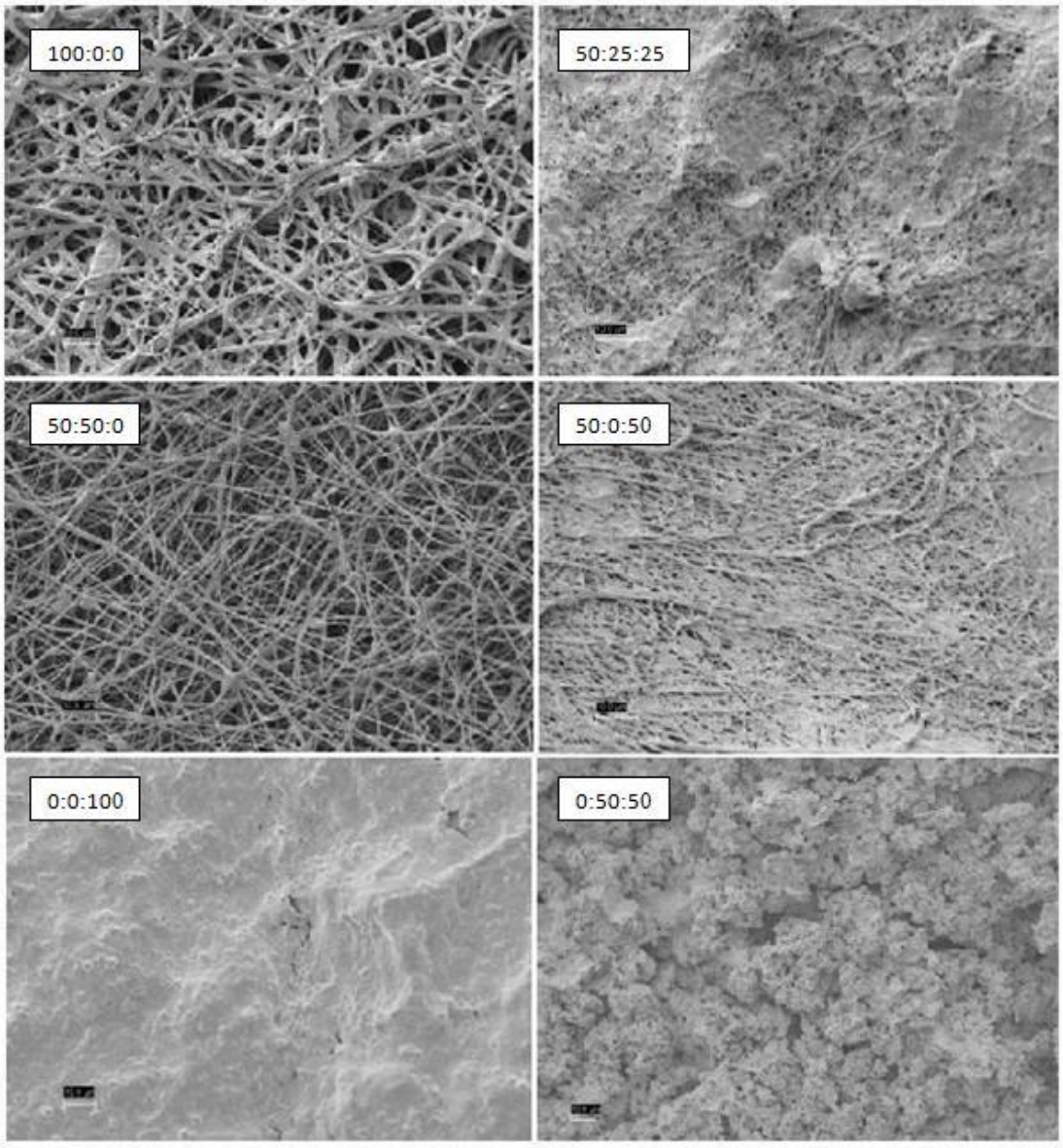

PDO:nHA:Fg Scaffolds Incubated in m-SBF for 5 days

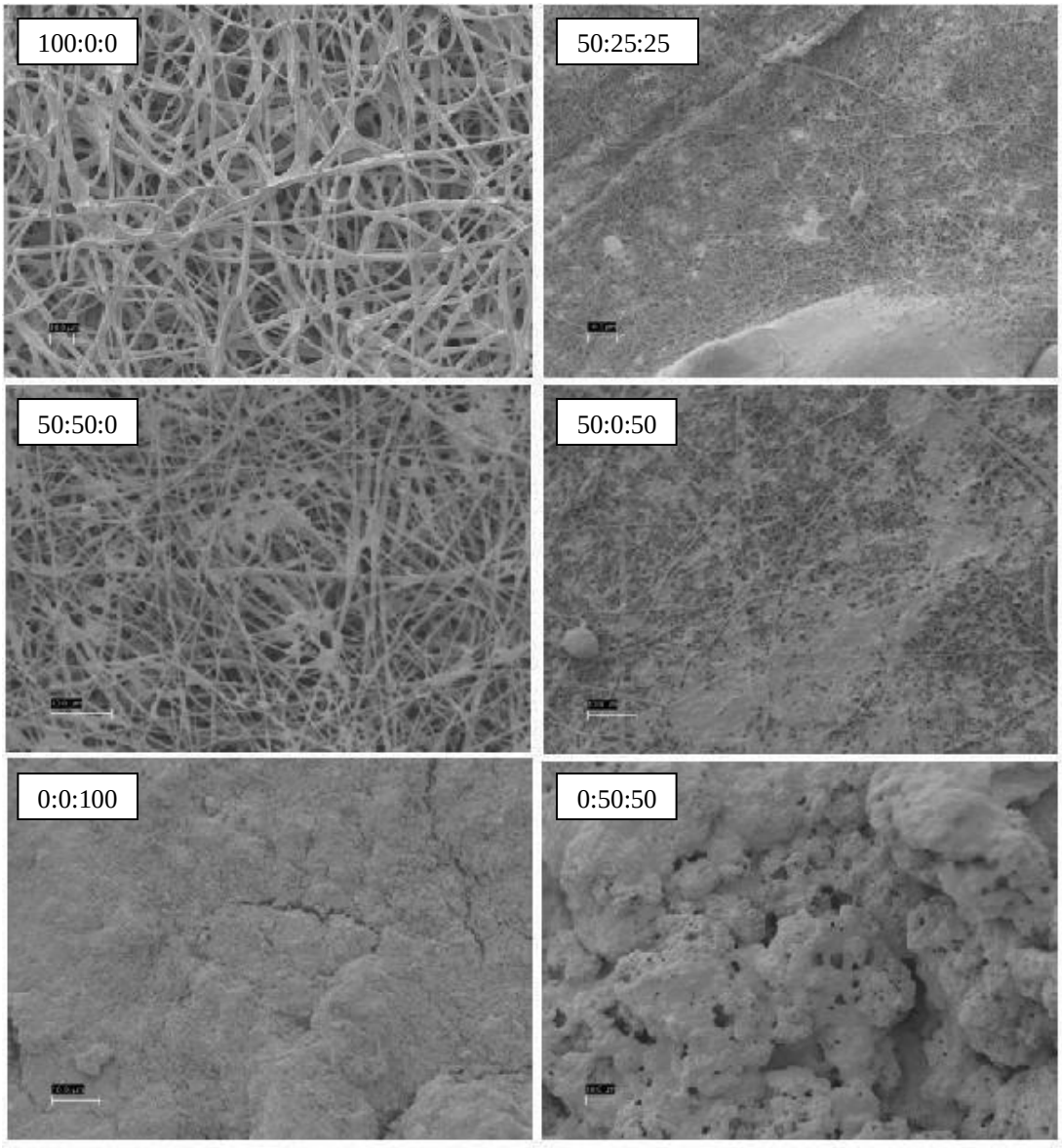

PDO:nHA:Fg Scaffolds Incubated in m-SBF for 14 days

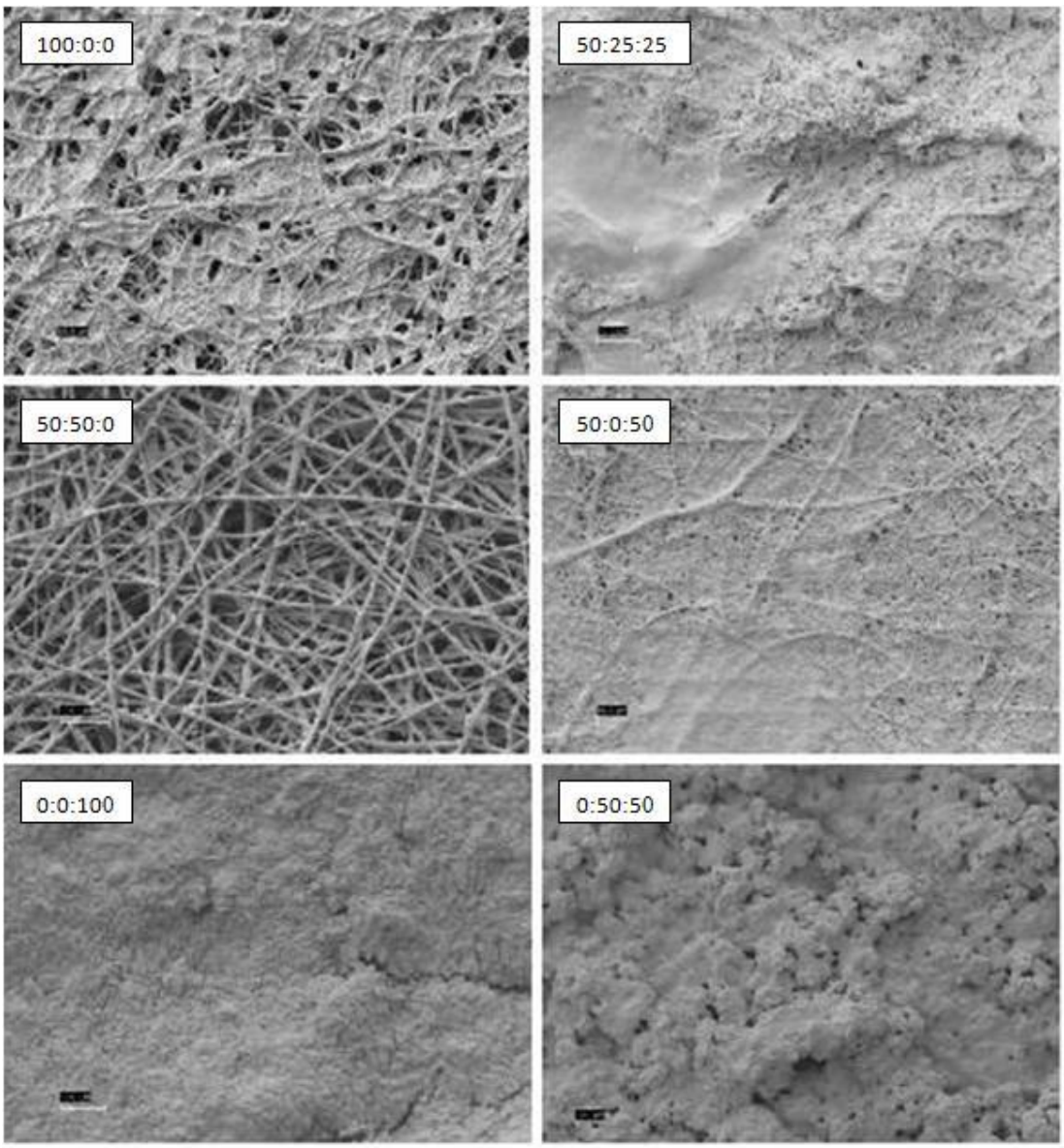

VITA

Isaac A. Rodriguez was born on April 29, 1985 in Fairfax, Virginia. He was raised in Fredericksburg, Virginia and graduated from Massaponax High School in June 2003. Isaac graduated from the University of Virginia in May 2007 where he earned a Bachelors of Science in Biomedical Engineering and an Engineering Business Minor. During his time at UVA he served as President for the Society of Hispanic Professional Engineers, President for the UVA Tae Kwon Do Club, Treasurer for La Unidad Latina, Lambda Upsilon Lambda Faternity, Inc., and a mentor for underclassmen in Biomedical Engineering. For his senior thesis project he and his group worked with a local biomedical Company, Barron Associates, in developing wireless physiological monitoring mechanisms. He is currently attending Virginia Commonwealth University in pursuit of his Ph.D. in Biomedical Engineering. He works in the Tissue Engineering Laboratory conducting experiments in the field of bone tissue engineering and is the second author to a manuscript published in Biomaterials titled "Multiple factor interactions in biomimetic mineralization of electrospun scaffolds." At VCU, he is also a co-founder and the Vice President of the American Society of Artificial Internal Organs: for young innovators and the alumni advisor to the Alpha Psi Chapter to La Unidad Latina, Lambda Upsilon Lambda Fraternity, Inc. Isaac also received the 2009-2010 Who's Who Among Students in American Universities and Colleges recognition at VCU.